Brain Stimulation 19 (2026) 103012

Contents lists available at ScienceDirect

Brain Stimulation

journal homepage: www.journals.elsevier.com/brain-stimulation

Hybrid optogenetic and electrical stimulation of retinal ganglion cells for artificial vision

William C. Kwan [a,b], Emma K. Brunton [a], Toon Goris [c], James M. Begeng [d], Tatiana Kameneva [d], Paul R. Stoddart [d], Michael R. Ibbotson [a], Rachael T. Richardson [e,f,g,1], Wei Tong [c,h,*,1]

[a] Department of Biomedical Engineering, University of Melbourne, Parkville, VIC, Australia
[b] Australian Regenerative Medicine Institute, Monash University, Clayton, VIC, Australia
[c] School of Physics, University of Melbourne, Parkville, VIC, Australia
[d] School of Engineering, Swinburne University of Technology, Hawthorn, VIC, Australia
[e] The Bionics Institute, East Melbourne, VIC, Australia
[f] The Department of Surgery (Otolaryngology), University of Melbourne, Parkville, VIC, Australia
[g] Medical Bionics Department, University of Melbourne, Parkville, VIC, Australia
[h] Graeme Clark Institute, University of Melbourne, Parkville, VIC, Australia

A B S T R A C T

Introduction: Millions of adults worldwide experience severe visual impairment due to photoreceptor loss from retinal diseases such as retinitis pigmentosa and macular degeneration. Retinal prostheses that provide artificial vision by stimulating the surviving retinal ganglion cells (RGCs) have emerged as a promising therapy. However, all clinically approved retinal prostheses that use electrical stimulation face the issue of electrical spread. As such, the quality of restored vision provided by existing devices has been limited. Optogenetic approaches provide greater spatial precision, however, they have poor temporal properties compared to electrical stimulation.

Materials and methods: We developed an opto-electrical hybrid approach and surveyed this stimulation strategy in the retina of two animal models: normal-sighted transgenic mice that express ChR2-H134R in a sub-population of RGCs and the degenerated retina of Royal College of Surgeons rats with residual RGCs transduced with ChrimsonR. We conducted whole-cell patch clamp recordings and measured calcium transients with the biosensor GCaMP7s to determine single-cell and population responses to hybrid stimulation, respectively.

Results: Hybrid stimulation reduced both electrical and optogenetic activation thresholds. Optical thresholds could be halved with electrical supplementation and synergistically, the opto-electrical coupling reduced the electrical intensity requirements to elicit action potentials by ~50 % ($p < 0.0001$). Additionally, hybrid stimulation evoked significantly higher firing frequencies, by an order of up to 2×, when compared to electrical or optical-only methods ($p < 0.0001$). These properties of hybrid stimulation were replicated in the diseased retina, where the reduced activation thresholds contributed to significantly reduced spread of activation compared to electrical stimulation alone ($p < 0.05$), a challenge that persists in devices that utilize extracellular electrical stimulation. Hybrid stimulation improved the spatial resolution of RGC activation when applied at retina-electrode spacing reflective of current epiretinal and suprachoroidal devices.

Conclusion: Combining the optogenetic and electrical modes of activation enabled significant reductions of each component in the stimulus, leading to more localised stimulation when compared to electrical-only stimulation, while also reducing the optical intensity required for optogenetic activation. Together with improvements in response reliability, hybrid stimulation may not only improve the resolution and refresh rate of future visual prostheses but may also provide greater control in neuromodulation for any bionic device that interfaces with neural tissue.

1. Introduction

Retinal degeneration is the leading cause of blindness in industrialised countries [1]. Retinal diseases that result in photoreceptor degeneration are some of the most prevalent retinopathies. Among them, age-related macular degeneration accounts for approximately 9 % of blindness globally and the inherited disease, retinitis pigmentosa, has a prevalence of 1:4000 [2,3].

Retinal prostheses aim to compensate for photoreceptor loss by stimulating surviving higher-order neurons, such as retinal ganglion cells (RGCs) or bipolar cells, through exogenous stimulation. This stimulation is typically conducted through charge injection from

* Corresponding author. School of Physics, University of Melbourne, Parkville, VIC, Australia.
E-mail address: wei.tong@unimelb.edu.au (W. Tong).
[1] These authors contributed equally as senior authors.

https://doi.org/10.1016/j.brs.2025.103012
Received 25 August 2025; Received in revised form 4 December 2025; Accepted 18 December 2025
Available online 23 December 2025

surgically implanted electrode arrays. There have been some promising developments surrounding electrode-based devices. Some devices that have been surveyed in animal models have the potential of restoring visual acuity up to 20/100 [4], a level that is above the threshold for legal blindness, which is 20/200. In devices tested clinically, electrode based prostheses have restored the ability of patients to perceive light, objects and movement. Implant recipients report improvements in their quality of life, ability to navigate their surroundings, social interactions, and ability to perform daily activities [5]. A significant limitation of all devices that have received US and European regulatory approval to date is their low spatial resolution, which is caused by issues such as electrical current spread. Currently, the highest visual acuity reported from a retinal prosthesis is from the PRIMA Implant (Pixium Vision, France) [6]. Initial observations in the early stages of the clinical trial saw the highest level of restored visual acuity was 20/460. However, with appropriate rehabilitation and training over many years, a longitudinal reassessment of patients who received the PRIMA implant showed marked improvements in their visual capabilities, developing the ability to read letters numbers and words with recipients achieving visual acuity of 20/135. With the addition of digital zoom enhancement provided by PRIMA glasses, participants could read smaller fonts at a size which is comparable to a visual acuity of 20/42 [7,8].

Implantation of electronic retinal prostheses requires complex and expensive surgeries and comes with potential complications, such as inflammation, making them suitable only for select groups of patients. In a longitudinal assessment of the PRIMA device, 26 adverse serious events occurred in 19 of the 32 participants. These events were non life-threatening and could be treated with surgical intervention [8]. To date there have been 13 devices developed. Six devices are still undergoing clinical trials and four have been discontinued [9]. Therefore, despite over ten devices reaching clinical trials, electronic retinal prostheses have not replicated the commercial or clinical successes of other neural prostheses, e.g. cochlear implants and deep brain stimulation [10]. We aimed to explore alternative strategies to overcome the challenges of restoring vision in cases of retinal degeneration.

In recent years, optogenetic based therapies have garnered significant attention. With optogenetics, light sensitive proteins (opsins) such as channelrhodopsin (ChR) are expressed on neurons, permitting neural circuit activation or silencing through the application of visible light. The exceptional level of spatial precision that comes with optogenetics has led to multiple potential therapeutic applications [11]. Given the unique optical accessibility of the retina, optogenetics has the potential to be implemented with less surgical invasiveness than electrical neural prostheses and thus is an attractive therapy for vision restoration.

Several studies have explored the restorative capacity of retinal optogenetic stimulation. In rd1 mice that are blind due to an inherited rod photoreceptor dystrophy, there have been demonstrations of surviving RGCs being transduced with ChR variants. Photoactivation of opsin-expressing RGCs activates visual pathways and has been shown to restore visually guided locomotion [12–14].

In nonhuman primate models, optogenetic stimulation of RGCs transduced with the ChR variant ChrimsonR could drive signal transmission all the way to the primary visual cortex, with the pathway being amenable to optical modulation for over a year [15,16]. In macaques, the spatial resolution of optogenetic RGC stimulation translated to a visual acuity of 20/249 [17]. In a promising clinical study, a 58-year-old patient who underwent adeno-associated virus (AAV) transduction of RGCs with ChrimsonR showed remarkable vision improvement. Prior to optogenetic therapy, the patient was only able to detect the presence of light. With optogenetic therapy, the patient gained the ability to identify and reach out to objects ($\sim$10 $\times$ 10 visual degrees object size) and execute visuomotor reaching tasks [18]. With careful consideration of the AAV serotype, opsin variant and the transduction strategy, optogenetics has the potential to restore vision to an acuity of 20/72, according to a modelling study [19].

Optogenetic-based visual prostheses suffer from two primary challenges. First, the light intensity required to activate opsins is significantly brighter than ambient light. Clinical investigations observing the effects of long-term exposure to intense light stimulation in neurons are limited and hence, there are unresolved concerns regarding long-term patient safety. As many studies driving neural activity use optical intensities that exceed the prescribed retinal safety limit, it is important to seek alternative methods to reduce the intensity of light required for effective neuromodulation. Second, the reliability of responses to optogenetic stimulation is inferior to that of electrical stimulation, which limits the stimulation rates that can be applied. Specifically, the amplitude and probability of responses are reduced during repeated stimulation [20], which may lead to image fading in patients. RGCs transduced with channelrhodopsin2 (ChR2) or one of its red shifted variants ReaChR have been shown to reliably respond to optogenetic stimulation frequencies up to 30 Hz [13,21,22]. This is far below the response rate of some RGCs, which discharge at $\sim$40 Hz in response to luminance changes [23] or >100 Hz in response to motion stimuli [24]. A key reason for this limitation is the rapid desensitisation and relatively long inactivation time constants for most opsins, typically tens of milliseconds for most ChR2 variants [25,26]. Ultrafast opsins with shorter inactivation time constants have been engineered to provide higher spike probabilities at stimulation rates up to 500 Hz. Unfortunately, they also require higher-intensity light, which carries the risk of phototoxic damage [27,28].

One method to reduce the optical power requirements for neuronal activation is to incorporate electrical supplementation. With appropriate tuning of optical and electrical power, a hybrid opto-electrical technique has the capability of retaining a high level of spatial precision in neural activation, characteristic of optogenetics, while improving the response reliability. The concept of optogenetics-based hybrid stimulation was first established in the cochlea [29–32] and sciatic nerve [33]. The addition of light reduced the electrical current required for activation, thus significantly reducing the spread of activation compared to electrical-only stimulation [31]. Additionally, hybrid stimulation increased the likelihood that a cell would respond to repetitive high-frequency stimulation [30,31]. Recently, hybrid stimulation in the glymphatic system of the brain was employed to restore aquaporin polarization in astrocytes, which improved recovery following ischaemic stroke [34]. In the retina, Roh and colleagues coupled electrical stimulation with optogenetic stimulation to elicit higher spike frequency in RGCs expressing ChR2-H134R than either stimulation modality alone, but the impact on spike probability in blind rd10 mice was significantly less evident, and the impact on the spread of activation was not explored [35]. Since the retina is intrinsically more complex than the cochlea or sciatic nerve, containing a greater diversity of neuron types and requiring two-dimensional control of neurons to generate images, a detailed study of hybrid stimulation and its effect on RGCs on a population level across two-dimensions is required.

Here, within the visual system, we explore the potential of hybrid electrical and optogenetic stimulation as a novel approach to restoring vision. Using a transgenic mouse model with ChR2-H134R expression in RGCs, we explanted the retinae to perform whole-cell patch clamp recordings of RGCs and assessed their activation thresholds and temporal responses to repetitive stimulation at different frequencies using hybrid, electrical or optogenetic stimulation. Furthermore, to study how RGCs in a degenerative retina respond to hybrid stimulation at a population level, we recorded calcium transients in RGCs transduced with ChrimsonR and GCaMP7s in Royal College of Surgeons (RCS-p+) rats, an animal model of retinitis pigmentosa. The primary goal of this study was to establish proof-of-concept for improving artificial vision using minimally invasive techniques. We investigated how hybrid stimulation (broad electrical combined with focused optical) could serve as an alternative stimulation modality for electrical-only devices and by extension, determine the translational utility of hybrid stimulation. As a new frontier of optogenetic-based therapies emerges, opto-electrical hybrid stimulation could contribute to improved delivery of artificial

vision and serve as a pioneer for the intersection between gene therapy and bionics.

2. Methods

2.1. Animals

All procedures performed in this study were in accordance with the ethical standards of the Animal Care and Ethics Committee of the University of Melbourne (Ethics ID# 21886). Mice with RGCs expressing ChR2(H134R) were obtained as a breeding derivative of COP4*H134R/EYFP mice (Jax strain 012569: B6; 129SGt(ROSA)26Sortm32(CAG-COP4*H134R/EYFP)Hze/J) and Cre-parvalbumin mice (Jax strain 008069:B6; 129P2-Pvalbtm1(cre)Arbr/J). Male and female mice aged 7–11 weeks (n = 21) were used in this study and were sourced from St Vincent's Hospital Biological Resource Centre, Australia.

For experiments investigating hybrid stimulation in reducing the spread of activation, Royal College of Surgeons (RCS-p+) rats (6 females, 5 males) aged 13–19 weeks were sourced from Ozgene, Australia. These rats were first anaesthetised via intraperitoneal injection of a mixture of ketamine (65 mg kg^{-1}) and xylazine (5 mg kg^{-1}). Depth of anaesthesia was confirmed via loss of response to a noxious toe pinch. Following this, a local anaesthetic eye drop (0.5 % proxymetacaine) was administered. In each eye, 3 μl of AAV2-Syn1-ChrimsonR-tdT (7.29×10^{13} GC ml^{-1}) or a [1:1] cocktail of AAV2-Syn1-ChrimsonR-tdT (7.29×10^{13} GC ml^{-1}) and AAV2-Syn1-GCamP7s (1.06×10^{13} GC ml^{-1}) was introduced via intravitreal injection, in a method as previously described by Puthussery & Fletcher [36]. In brief, a 32G needle is inserted through the sclera, approximately 1 mm posterior to the limbus, at a 45° angle to avoid damage to the lens. The needle was connected to a 10 μl Hamilton syringe (Model 701N) via silicon tubing to facilitate the injection. Post injection, an antibiotic eye ointment (tobramycin) was applied. Animals were then recovered for a minimum of 3 weeks to accommodate viral transduction before the animals were euthanised and dissection of retinal tissue occurred.

2.2. Retinal preparation

Animals were anaesthetised via an intraperitoneal injection of a mixture of ketamine (100 mg kg^{-1}) and xylazine (10 mg kg^{-1}). After the depth of anaesthesia was confirmed via lack of response to a noxious toe pinch, the eye was enucleated and bathed in carbogenated Ames' medium (Assay Matrix) supplemented with 23 mM $NaHCO_3$ and bubbled with 95 % O_2/5 % CO_2 at room temperature. Following the enucleation, the animal was humanely killed via an intracardiac injection of pentobarbital.

Post enucleation, an incision was made in the cornea, and the subsequent dissection was undertaken in Ames' medium. The eyes were hemisected behind the ora serrata followed by lensectomy and vitrectomy. The sclera and retinal pigment epithelium were removed before radial incisions were made to flatten the retina. These retinal whole-mounts were placed with the ganglion side up in a recording chamber (Warner Instruments) while being superfused with the carbogenated Ames' medium (2–3 ml/min). Visualization of the tissue was undertaken on a fixed-stage, upright microscope (Olympus cat# BX61WI).

2.3. Whole-cell patch clamping

Whole-cell patch clamping was conducted on RGCs expressing ChR2 (H134R) from mouse retina. RGCs with ChR2(H134R) were identified through their co-expression of EYFP, using a 40x water immersion objective (Olympus cat# N2667700) and a GFP filter (Olympus cat# U-MNIBA3). Cells were visualised with a monochrome digital camera (Olympus XM-10) and μManager software [37]. Individual RGC responses were recorded under current clamp conditions, as described previously [38]. Borosilicate micropipettes (8–10 MΩ) were prepared using a CO_2 laser puller (Sutter instruments Cat# P-2000) and filled with 6 μL of fluorescent intracellular solution that consisted of (in mM) 125 K-Gluconate, 2 $CaCl_2$, 2 $MgCl_2$, 10 HEPES, 10 EGTA, 2 Mg-ATP, 0.5 Na_2-GTP and 0.125 Alexa Fluor 594. To obtain access to a cell, a small tear was made in the retinal inner limiting membrane with a micropipette (3–4 MΩ) controlled by a micromanipulator (Sutter Instruments Cat# MPC-325). Upon successful tear and clear access to a ChR2 (H134R) RGC, a freshly prepared recording micropipette filled with intracellular solution was lowered into the extracellular bath. Prior to recording, the pipette resistance was compensated with a bridge balancing circuit on the amplifier (NPI, BA-1S). Membrane potentials were amplified (BA-1S, NPI) and digitised with 16-bit precision at 20 kHz (USB-6221, National Instruments). Instrument control and recording of membrane potentials were performed using custom MATLAB software.

When a whole-cell configuration was achieved, depolarizing and hyperpolarising current between −200 pA and 200 pA was delivered in 20 pA current steps to obtain baseline intrinsic properties of the cell. Following the recording of the cell's intrinsic properties, the patched RGC in whole-cell configuration was prepared for optogenetic stimulation. To ensure RGC responses were a direct result of stimulating ChR2-H134R expressing RGCs and not from photoreceptor input, synaptic input to RGCs was eliminated by washing in a synaptic blocker cocktail consisting of (in mM) 0.01 NBQX, 0.05 D-AP5, 0.02 L-AP4, 0.1 picrotoxin and 0.01 strychnine. This blocked di-synaptic photoreceptor input to RGCs [39]. For optical stimulation, a 488 nm laser light source (Optotech) was used, projected down the optical axis of the microscope and focused to a spot size of 35 μm by the microscope objective at the sample plane. Electrical stimulation was delivered intracellularly via the patch microelectrode.

We adapted our stimulation protocols and definitions of stimulation thresholds from the work of Soto-Breceda and colleagues [40]. To determine the electrical activation thresholds, 10 stimulus pulses at a 2 Hz repetition rate were delivered to the cell across a range of amplitudes. To calculate optical threshold levels, 10 light pulses at a 2 Hz repetition rate was delivered at power levels between 0 and 2.78×10^{21} photons cm^{-2} s^{-1}. The stimulus amplitude during the 2 Hz stimulation pulse trains which elicited a response rate of 50 % was defined as threshold and the minimum amplitude that could evoke 100 % response reliability was defined as saturation (Fig. 2a).

To study the impact of hybrid stimulation on stimulation threshold, optical and electrical stimulation were delivered to RGCs (n = 11) using pulse durations of 10 ms and 3 ms, respectively. These stimulation pulses were delivered either simultaneously, or sequentially with electrical pulses being immediately after optical stimuli. Stimulation was delivered via both optical and electrical modalities was delivered at 11 different amplitudes, including a zero-amplitude setting, in a random sequence at a frequency of 2 Hz. Therefore, this approach resulted in the evaluation of 121 unique stimulus combinations, with each combination being repeated 10 times (Fig. 2b). We defined the threshold as the amplitude that would elicit 50 % response reliability, as determined by a sigmoidal fitting. This stimulation paradigm was employed to generate the data presented in Fig. 2. To study the impact of hybrid stimulation on temporal response reliability, optical and electrical stimulation were delivered using pulse durations of 1 ms and 3 ms, respectively. The stimulation was sustained for 3 s at repetitive frequencies of 2, 20, 50 and 200 Hz. The amplitude used for all stimulation frequencies was threshold and supra-threshold for electrical and optical stimulation respectively. Thresholds were defined during stimulation at 2 Hz. This stimulation paradigm was employed to generate the data presented in Fig. 3. For all temporal study experiments, electrical pulses were delivered immediately after optical stimulation (Fig. 3a).

Similar experiments were also performed on RGCs expressing ChrimsonR from RCS-p + rat retina. We investigated the effects of hybrid stimulation on stimulation threshold (n = 4) and temporal response (n = 5) using optical and electrical stimulation with pulse

durations of 1 ms and 3 ms, respectively. Optical stimulation was delivered using a 595 nm LED (M595F, Thorlabs) projected and focused as described above. In the hybrid stimulation protocol, electrical pulses were delivered immediately after optical stimuli. This stimulation paradigm was used to generate data for Figs. S2 and S3. Additionally, one RGC was stimulated using an in-house 80 μm diameter platinum electrode placed epiretinally above the ILM, about 50 μm away from the recorded cell. Electrical stimulation was delivered using anodic-first biphasic pulses with a pulse duration of 0.5 ms. This generated Fig. S4.

2.4. Morphology reconstruction and cell type identification

Images of RGCs, backfilled with Alexa Fluor 594 hydrazide during recording experiments, were acquired on a confocal microscope (Olympus cat# FV1200). Following acquisition of the RGC morphology, the retained sample was counterstained with 100 μM sulforhomadine-101 in Ames' media for 5 min to provide delineation of the retinal layers. Z-stacks of images from the GCL to the inner nuclear layer were acquired at a resolution of 1024 × 1024 with a step size of 1 μm. Adjustments to image contrast and brightness were performed on Adobe Photoshop 2023 or FIJI [41].

The diameter of the dendritic field and soma was measured using FIJI. To determine whether RGCs were ON, OFF or ON-OFF sub-types, the depth within the IPL where the dendritic field terminated was measured as previously described by Famiglietti Jr & Kolb [42]. Using the GCL/IPL boundary as reference point 0 % and the INL/IPL boundary as 100 %, RGCs with dendritic arbours that terminated at a depth of <60 % were deemed to be ON-cells.

2.5. Viral vectors

Plasmids encoding ChrimsonR and GCaMP7s were procured by Addgene before being cloned and packaged into AAV2 vectors by VectorBuilder. pAAV-Syn-ChrimsonR-tdT was a gift from Edward Boyden (Addgene plasmid #59171; http://n2t.net/addgene:59171; RRID: Addgene_59171) [20]. pGP-AAV-syn-jGCaMP7f-WPRE was a gift from Douglas Kim & GENIE Project (Addgene plasmid # 104488; http://n2t.net/addgene:104488; RRID: Addgene_104488) [43].

2.6. Calcium imaging

Calcium imaging was performed on retinal flatmounts which underwent AAV-mediated transduction of ChrimsonR and GCaMP7s within the GCL in RCS-p + rats (n = 12). Using a confocal microscope (Olympus, FluoView FV1200) equipped with 20 × and 40 × water-immersed objectives, images were recorded at a frequency of 4.6–7.8 Hz. Each image covered an area of approximately 318 × 318 μm or 159 × 159 μm. Images covering different regions of the retina were taken in response to each stimulus, and subsequently stitched together using the MosaicJ plugin [44]. Stimulation was delivered using either (i) focused optical and broad electrical stimulation (n = 9) for Fig. 4, S5-7, or (ii) focused electrical and broad optical stimulation (n = 3) for Fig. S8.

Optical stimulation was delivered through an LED coupled optical fibre (595 nm, M595F, Thorlabs), with the fibre tip cleaved. Each optical stimulus had a pulse duration of 1 or 10 ms. Optical stimulation was delivered with the fibre tip positioned on or near the retinal flat mount. The optical fibre illuminated either a focused area with a diameter of 125 μm or a broad region of the retina.

For electrical stimulation, we used an in-house platinum-iridium wire insulated with a glass pipette as previously described by Yunzab and colleagues [45]. The electrode was placed epiretinally on the surface of the retina. Broad electrical stimulation was delivered using 127 μm electrodes placed around 0.5 mm above the retina (n = 5). The exposure length of platinum-iridium wire was estimated at 2 mm, leading to an effective surface area of 500 μm in diameter and an impedance of 4 kΩ. This generated Fig. 4e–h and S5-7. In another set of experiments (n = 4), the electrode was coated with PEDOT:PSS to enhance their charge injection capacity and placed 3 mm above the retina. Focused electrical stimulation was delivered using a 20 μm electrode in contact with the retina. The exposure length was minimal, and the electrode impedance was over 100 kΩ. This generated Fig. 4e and i. A silver/silver chloride wire was placed approximately 2 cm away from the stimulating electrode in the chamber and used as a distant electrical return electrode. Electrical stimulation was delivered using a Grapevine Neural Interface System and a Nano2 + Stim or Macro2 + Stim headstage (Ripple Neuro, USA). Each electrical stimulation consisted of anodic-first biphasic pulses, with a pulse duration of 500 μs with no inter-pulse-interval, or a pulse duration of 200 μs and inter-pulse-interval of 33 μs. For hybrid stimulation, electrical pulses were delivered immediately after each optical stimulation. For all stimuli (optical, electrical and hybrid), stimulation was delivered as a repetitive pulse train at a frequency of 50 Hz. Each train consisted of 100 pulses, and the amplitude was adjusted every 20 s.

Cell activity was measured by first manually identifying the location of each RGC soma using the Region of Interest Manager in ImageJ (Fiji). Then custom MATLAB scripts were used to measure the change of fluorescence (ΔF/F) of each cell. A cell was considered activated if ΔF/F exceeded a threshold within 3 s of stimulus onset. The threshold was defined as either 0.2 or 3 times the standard deviation, whichever was larger, as previously described [46].

We first defined the stimulation threshold based to the evoked activity in a 159 μm × 159 μm imaging frame that included the optical fibre within its field of view. The suprathreshold was defined as the point at which the activation pattern or the number of activated cells did not increase when the amplitude of optical-only or electrical-only stimulation increased. This was assessed visually during the experiment. Three different optical (O-1, O-2, O-3) and three different electrical (E-1, E-2, E-3) stimulus levels were then used to study the impact of hybrid stimulation. O-3 was at a supra-threshold level, which was up to about 9.8 × 1017 photons cm^{-2} s^{-1}, while E-3 was at a supra-threshold level, which was up to 0.9 mA. Compared to the patch clamping experiments where illumination was delivered via objectives, the measurement of illumination intensity is less accurate in these calcium imaging experiments, as the placement of the optical fibres was difficult to control. In Fig. 4, Optical was denoted as O-3/E-off, Electrical as O-off/E-3, and Hybrid as O-2/E-2.

For each animal, the number of RGCs and the area activated were quantified. The area of the activated retina was measured by finding a 90 % confidence area ellipse around the active cells. The localisation index was defined by calculating the percentage of activated cells within a given area. For each retina, this given area was measured by finding a 90 % confidence area ellipse around the cells activated at O-3/E-off.

2.7. Histology

The protocol for immunofluorescent labelling of the retina has been adapted from Hendrickson and colleagues [47]. Retinae were fixed in 4 % paraformaldehyde in 0.01 M PBS for 24 h at 4 °C. Following fixation, they were washed in 0.01 M PBS. To prepare retina sections, the tissue was placed in a [1:1] solution of OCT (Tissue Tek) and 30 % sucrose in PBS for 16 h. Retinae were then placed in a cryomold, embedded with OCT, and the samples were snap frozen in 2-methylbutane that had been chilled to −50 °C for 2 min. Samples were then cut in the transverse plane on a cryostat (Leica #CM3050S) at a thickness of 20 μm. Sections were mounted directly onto Superfrost Plus® slides and stored at −20 °C.

To delineate the layers of the retina, sections were counterstained with Hoechst 33258 (Life Technologies #H3569, 1:1000). Sections were immunolabelled with an antibody against GFP (Abcam #ab13970, 1:2000) to amplify the signal of the ChR2(H134R)-YFP and GCaMP7s cells, against parvalbumin (Swant #PV27, 1: 3000) as a proxy for quantifying the number of RGCs expressing ChR2-H134R in mice retinae

and an antibody against mCherry (Rockland #600-401-P16, 1:1000) to amplify ChrimsonR signal in RCS-p+ retina samples. Secondary antibodies against chicken conjugated to Alexa Fluor 488 (Thermo Fisher # A11039, 1:1000) were used to visualise anti-GFP label whilst antibodies against rabbit conjugated to Alexa Fluor 594 (ThermoFisher # A32754, 1:1000) were used to visualise cells parvalbumin and ChrimsonR expressing cells. Images from transverse sections were acquired on a wide field Leica Thunder Imager microscope using a 20× objective.

2.8. Data and statistical analysis

Our primary measure of the efficacy of a stimulation modality was the response rate, defined as the percentage of pulses that elicited action potentials. Action potentials were detected by threshold crossings at −20 mV, confirmed through visual validation of the stimulus artefact. For each stimulus level, we assessed the response efficacy by fitting a sigmoid function

$$f(x) = \frac{a}{1 + e^{-b(x-c)}} \quad [1]$$

in which f(x) is the response rate and x is the amplitude of electrical or optical stimulation. Here, coefficient b represents scaling factors that determine the saturation amplitudes, a represents the gain of the sigmoidal curve, and c represents the thresholds (50 % of the saturation level).

For threshold analysis experiments, we estimated optical thresholds at each level of electrical stimulation and vice versa for each cell. In our population analysis, hybrid threshold values were normalised to those observed under sole electrical or optical stimulation. Data from cells exhibiting over 50 % response rate even at the lowest stimulation levels were excluded from the population analysis. We then categorized the threshold values into four groups based on normalised stimulation levels: 10–30 %, 30–50 %, 50–70 % and 70–90 %, facilitating comparative analysis. Two-way analysis of variance (ANOVA) with post hoc multiple Tukey comparisons was used to quantify the effects of hybrid stimulation on optical/electrical thresholds and response reliability ($p < 0.05$ was considered significant; GraphPad Prism).

For temporal analysis experiments, each cell was stimulated with the three stimulation modalities as described above at repetition rates of 2 Hz, 20 Hz, 50 Hz and 200 Hz repetition rates. The duration for each pulse train was 3 s and delivery of stimulation at the four frequencies and three stimulation modalities (12 conditions) constituted one trial. Cells included in this study underwent a minimum of three trials. The number of action potentials elicited during stimulation pulse delivery (e.g. 150 pulses during 3 s of 50 Hz stimulation) was used as a measure of response reliability. The response reliability was expressed as a percentage and averaged (mean) across all trials. Response latency was determined by the time it took from the onset of each stimulus to the peak of the first action potential. Specifically, for optogenetic-only stimulation, latency was defined as the time from light onset to the first action potential. For electrical-only stimulation, latency was measured from current onset to the first action potential. For the hybrid stimulation, as the optogenetic stimulus was always delivered first, latency was defined from the onset of light illumination to the first action potential. Outliers were removed with the ROUT method (Q = 0.1 %; GraphPad Prism). Two-way analysis of variance (ANOVA) with post hoc multiple Tukey comparisons was used to quantify the properties of RGC responses to hybrid stimulation compared to optical-only and electrical-only stimulation across all four frequencies ($p < 0.05$ was considered significant; GraphPad Prism).

For calcium imaging experiments, the number of GCaMP7s expressing RGCs that responded to stimulation under optical, electrical or hybrid modalities, the areal spread of activation, and the localisation index were quantified with Wilcoxon Signed-Rank tests where statistical significance was determined when the p value was <0.05 (IBM, SPSS).

3. Results

3.1. A transgenic mouse model to explore hybrid stimulation in the retina

To examine the feasibility of hybrid stimulation as a novel method for modulating RGC activity, we crossed mice expressing parvalbumin-Cre with mice expressing Cre-dependent ChR2(H134R)-EYFP to generate animals with ChR2(H134R) in parvalbumin (PV) expressing RGCs. We performed a histological survey of retinae from our ChR2(H134R) mouse line to determine the extent of ChR2(H134R) expression in the retina.

The retina comprises five major neuronal subtypes, each organised within its laminar structure. Transmission of photic signals originates in the most superficial layers of the retina, the photoreceptors, before being di-synaptically relayed to the deepest layer, the ganglion cell layer (GCL), via bipolar cells in the outer nuclear layer. The cells within the GCL serve as the final outpost of visual information in the eye before it is transmitted to the brain via the optic nerve [48]. These layers can be readily delineated with a Hoechst counterstain. Analysis of horizontal cryo-sectioned tissue revealed that expression of ChR2(H134R) was confined to the GCL (Fig. 1a–c) and within parvalbumin expressing RGCs (Fig. 1d–g). The proportion of PV-ChR2(H134R) RGCs compared to the total RGC population was estimated to be ~30–40 % based on previous studies which quantified parvalbumin expression within the GCL [49,50].

RGCs are diverse and within the mouse over 40 subtypes have been defined based on their genetic, functional and morphological identities [51,52]. Broadly, in a functional context, RGCs can be segregated into three distinct populations based on their responses to light. The three types are 1) ON-cells that respond to brightness increments, 2) OFF-cells that respond to brightness decrements, and 3) ON-OFF cells that are responsive to both brightness increments and decrements [53]. Morphologically, in the mouse retina, RGCs are also subdivided into four groups aptly named A, B, C, and D RGCs. Classification is based on soma and dendritic field diameter as well as dendritic spine density. A, B and C groups possess both ON and OFF subtypes whereas RGCs in the D group are the ON-OFF subtype. During patch clamp recordings, RGCs were back-filled with a fluorescent tracer which permitted the reconstruction of the cells' dendritic arbour (Fig. 1h and i). The depth within the inner plexiform layer (IPL) where the dendritic arbour stratifies was used to phenotype each cell into one of the three main classes. Within our experiments we were able to study the effects of hybrid stimulation in both ON-cells and OFF-cells across all four morphological groups (Fig. 1j–l) (Tables S2–5). This aligns with previous observations that while PV expressing RGCs only encompass ~40 % of the total RGC population, there are ON, OFF and ON-OFF RGCs within the four major morphological groups that express PV [49].

3.2. Hybrid stimulation reduces electrical and optical thresholds

The spread of activation due to electrically evoked activity depends on the amplitude of stimulation. Previous studies have demonstrated that coupling electrical stimulation with optical stimulation significantly reduces the electrical current that is required to activate the sciatic nerve or neurons in the cochlea [30,31,54]. We wanted to determine if this hybrid approach could be translated to RGCs of the retina. In isolated whole-mount retinae, we recorded responses to hybrid stimulation in single RGCs in a whole-cell current clamp configuration. RGCs were electrically stimulated intracellularly during patch recordings, while 488 nm blue light pulses were delivered via a laser-coupled optical fibre, focused on the cell through the microscope objective. To ensure recordings were a direct result of optogenetic stimulation of RGCs, di-synaptic photoreceptor inputs to RGCs were sequestered through pharmacological synaptic blockade. For each cell, we first identified the thresholds for electrical and optical stimulation. We defined threshold as the stimulation amplitude required to elicit a

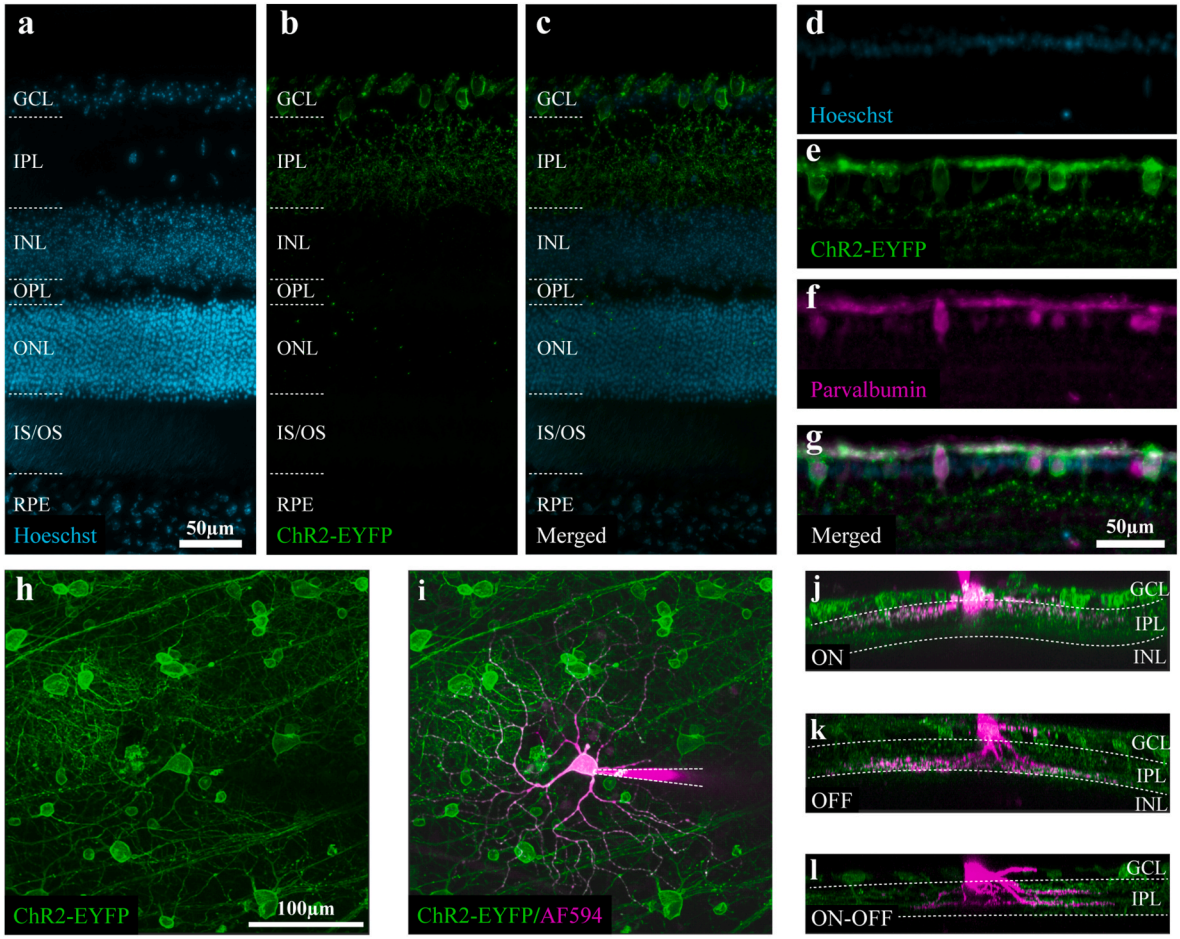

Fig. 1. Transgenic mouse model with ChR2(H134R) expression in RGCs.
(a) Lamination of the retina as revealed by Hoechst nuclear stain in horizontal cryosections **(b)** Distribution of cells expressing ChR2(H134R)-EYFP (green) within the retina. **(c)** Overlay of the Hoechst nuclear stain and EYFP reveals that expression of ChR2(H134R) is confined to cells within the GCL together with their extensions into the IPL. **(d–g)** Distribution of ChR2(H134R) expressing cells that co-express parvalbumin (magenta). **(h)** Distribution of ChR2(H134R) cells within the GCL (flatmount preparation). **(i)** An example of a RGC that has been backfilled with AF594 dye (magenta) from the patch microelectrode (dotted white outline) during recording. Examples of **(j)** an ON-cell **(k)** an OFF-cell and **(l)** an ON-OFF cell after back filling with AF594 dye. Abbreviations: GCL: ganglion cell layer; IPL: inner plexiform layer; INL: inner nuclear layer; OPL: outer plexiform layer; IS/OS: inner segment/outer segment; RPE: retinal pigment epithelium.

50 % response probability during the 2 Hz pulse train (5 s train duration). The minimum stimulation level that would evoke 100 % reliability was defined as the saturation threshold (Fig. 2a).

Once the thresholds were defined, 10 hybrid stimulation pulses were delivered at a rate of 2 Hz. Eleven linearly scaled steps between zero and saturation-threshold amplitudes for both electrical and optical stimulation were tested. Each optical step was paired with all 11 electrical steps in random order, creating 121 combinations (Fig. 2b and c). Optical pulse duration was 10 ms and electrical pulse duration was 3 ms, as used previously for hybrid stimulation of spiral ganglion neurons in the cochlea [30]. It has been reported that the timing of the opto-electrical coupling impacts the facilitation of the response. Delaying the delivery of electrical pulses relative to the onset of the optical pulses has been shown to be necessary to align the relatively slow change in membrane potential resulting from the opening of the ChR2-H134R channel with the very rapid action of sodium channels. Evidence of facilitation during hybrid stimulation can be seen as a reduction in electrical activation threshold, such that a greater reduction in threshold was observed when the electrical stimulus was delayed compared to simultaneous presentation of the stimuli in auditory neurons [30,54]. To explore this in the retina, hybrid stimulation was delivered with electrical pulses at delays of 0 ms or 10 ms. With an optical pulse duration of 10 ms, a 0 ms delay signifies simultaneous delivery and a 10 ms delay signifies sequential delivery (Fig. 2b and c). The anatomical characteristics of our recorded RGC population are summarised in Table S1. No significant differences in electrical and optical thresholds were exhibited between the RGC subtypes (Table S1). Therefore, data from all RGCs were pooled and analysed collectively.

We quantified the efficacy of hybrid stimulation to reduce activation thresholds by plotting optical and electrical thresholds as functions of the intensity of electrical and optical stimulation, respectively (Fig. 2d). Threshold levels were normalised to the thresholds obtained with electrical or optical-only stimulation. Incorporating electrical stimulation significantly attenuated optical thresholds compared to optical stimulation alone whereby a normalised 50 % intensity level reduced optical thresholds by ~50 % (Fig. 2e (Two-way ANOVA, $n = 15$, $p < 0.0001$),). In both the simultaneous and sequential conditions, the most apparent effect was seen when electrical stimulation was delivered at 50–70 % intensity relative to threshold. The optical threshold was approximately halved compared to optical stimulation alone (post hoc Tukey test, $p < 0.0001$), reduced from 2.41×10^{21} photons s^{-1} cm^{-2} to about 1.21×10^{21} photons s^{-1} cm^{-2}. This brings the optical threshold within the safe limit for 488 nm laser stimulation (estimated at 1.36×10^{21} photons s^{-1} cm^{-2}) [55]. Delaying the electrical stimulus by 10 ms provided no further significant reduction in optical threshold (Two-way ANOVA, $F[1,59] = 2.6$, $p = 0.1136$).

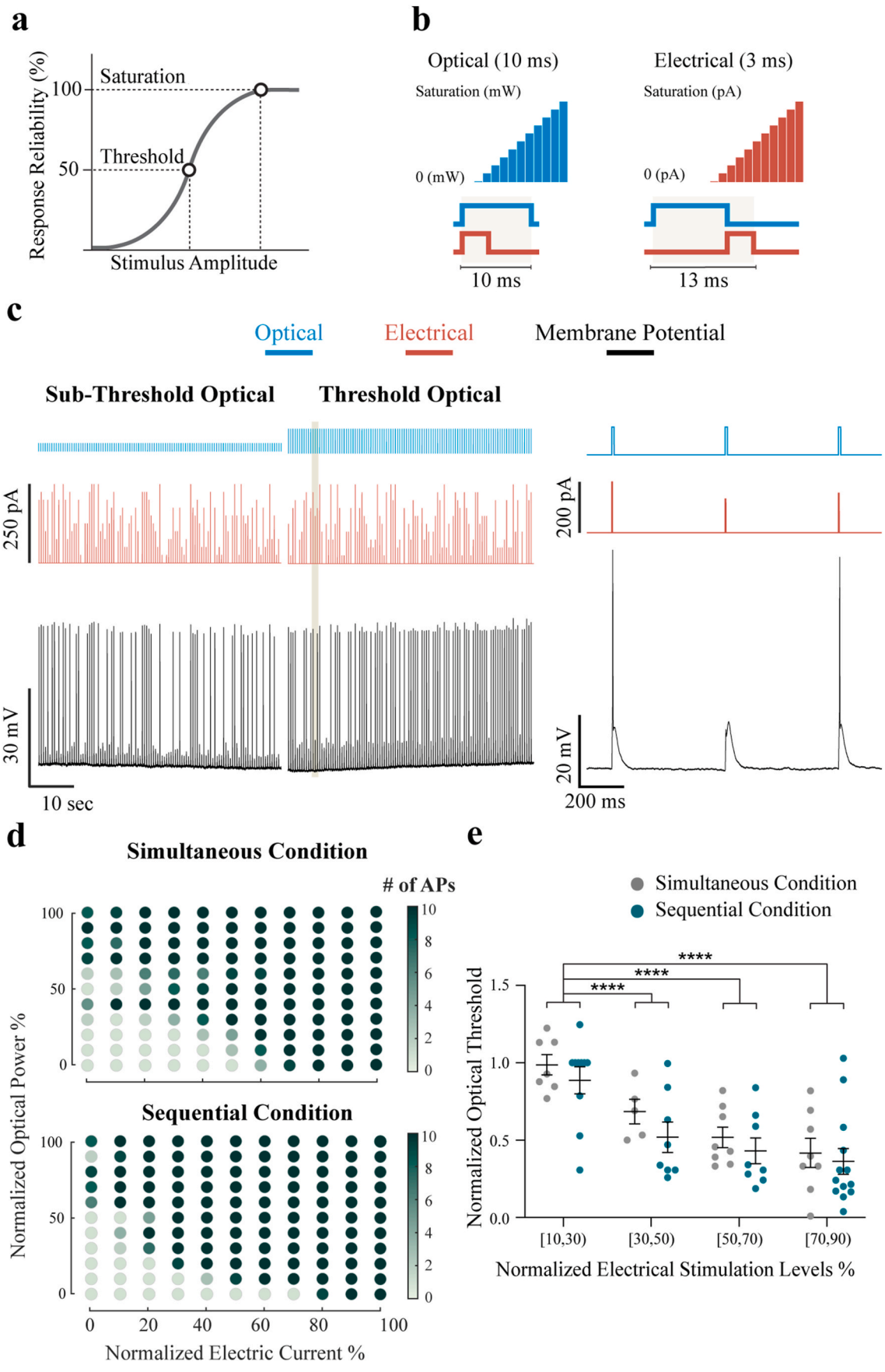

(caption on next page)

Fig. 2. Modulation of activation thresholds with hybrid stimulation in mouse ChR2-H134R RGCs.
(a) In whole-cell current-clamp configuration, a cell is stimulated electrically across a range of amplitudes to determine activation thresholds. The same is done for optical stimulation. Threshold and saturation thresholds were defined as the amplitudes that elicited response reliability of 50 % and 100 %, respectively. **(b)** Experimental protocol. A series of ten stimulation pulses at a 2 Hz repetition rate is delivered. Hybrid stimulation pulses were delivered either simultaneously (0 ms delay between optical and electrical pulses) or sequentially (electrical pulses delivered after optical pulses i.e. 10 ms delay). **(c)** Example traces of threshold testing where optical amplitude is fixed (blue) and electrical stimulus is presented between 0 and saturation amplitude in randomized order (red). The left-hand panel shows a membrane potential response trace (black) representing a recording with sub-threshold optical stimulus and the middle panel shows responses during a threshold optical stimulus. Note that more action potentials are generated with threshold optical stimulation. The right-hand panel displays a magnified view of the RGC membrane potential during electrical stimulation at varying amplitudes, coupled with optical stimulation at a threshold level (indicated by the shaded area in the middle panel). Note that the stimulation pulse in the middle of the trace failed to elicit an action potential. **(d)** An example cell highlighting the effects of hybrid stimulation on activation thresholds. Plots represent the number of action potentials (denoted in colour bar) that were elicited at varying optical and electrical amplitudes under hybrid conditions during the simultaneous condition (top) and sequential condition (bottom). Incorporating a delay did not significantly reduce activation thresholds. **(e)** Population analysis of the attenuation of optical thresholds with the addition of electrical current as per two-way analysis of variance (ANOVA). Data points represent recordings taken across all cells during hybrid stimulation. Data points where optical saturation was reached without electrical input were discarded. The number of cells which make up the data points are: [10,30) % simultaneous (n = 5); [10,30) % sequential (n = 6); [30,50) % simultaneous (n = 4); [30,50) % sequential (n = 6); [50,70) % simultaneous (n = 6); [50,70) % sequential (n = 6); [70,90) % simultaneous (n = 7) [70,90) % sequential (n = 9). Notably, electrical stimuli at a normalised 50 % intensity level reduced optical thresholds by ~50 % ($p < 0.0001$). No significant differences ($p = 0.1136$) were observed between the sequential and simultaneous conditions of hybrid delivery. Error bars represent the standard errors of the mean.

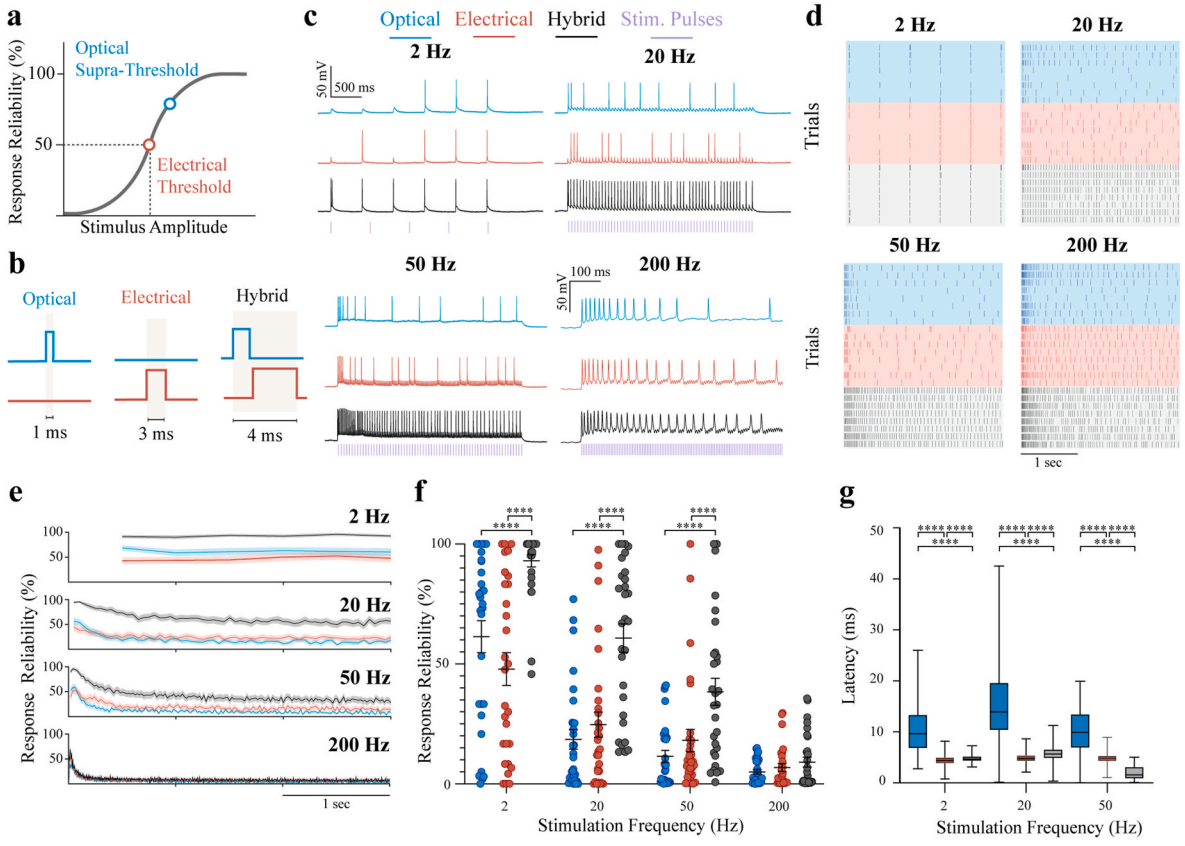

Fig. 3. Temporal dynamics of ChR2-H134R RGC responses to optical, electrical, and hybrid stimulation at varying frequencies.
(a) Ten stimulus pulses at a 2 Hz repetition rate delivered at intensities that elicited 0 %–100 % response rates were used to determine a RGC's response threshold to electrical and optical stimulation. **(b)** A schematic of the stimulus conditions used for examining response properties. RGCs were presented with optical-only stimulation (1 ms pulse width), electrical-only stimulation (3 ms pulse width), or hybrid stimulation (1 ms optical stimulus followed by 3 ms electrical stimulus with a delay of 1 ms from optical onset) at four frequencies (2 Hz, 20 Hz, 50 Hz, 200 Hz). **(c)** Whole-cell current-clamp recordings from a single cell that responds prolifically to hybrid stimulation. Raw traces from one trial consisted of stimulation under 12 conditions (i.e. the three different stimulation modalities at four tested frequencies. The scale bar for 2 Hz stimulation is the same for 20 Hz and 50 Hz. **(d)** Raster plots of all trials of the example cell as shown in **(c)**. **(e)** Population analysis of the decay in response reliability over the time-course of optical only, electrical only and hybrid stimulation. The solid line denotes the mean and the shading represents the standard error of the mean. **(f)** Population analysis of the mean response reliability and comparison of optical only, electrical only and hybrid stimulation. Mean response reliability is summarised in Table S7. Raw traces and raster plots from another cell representative of the mean response reliability are shown in Fig. S1. Hybrid stimulation response reliability was quantified as per two-way analysis of variance (ANOVA) with post hoc multiple comparison tests (n = 29). Hybrid conditions enhanced response reliability at stimulation frequencies up to 50 Hz ($p < 0.0001$). Error bars represent the standard errors of the mean and are summarised in Table S7. Exact p values for response reliability further summarised in Table S8. **(g)** Response latency of RGCs at stimulation frequencies where hybrid stimulation enhanced response reliability. Response latency following stimulation was quantified as per two-way analysis of variance in the same RGC population presented in **(f)**. Latencies were significantly different between each stimulation modality at all frequencies ($p < 0.0001$). Median values, standard deviations, and exact p values are further summarised in Tables S9 and S10.

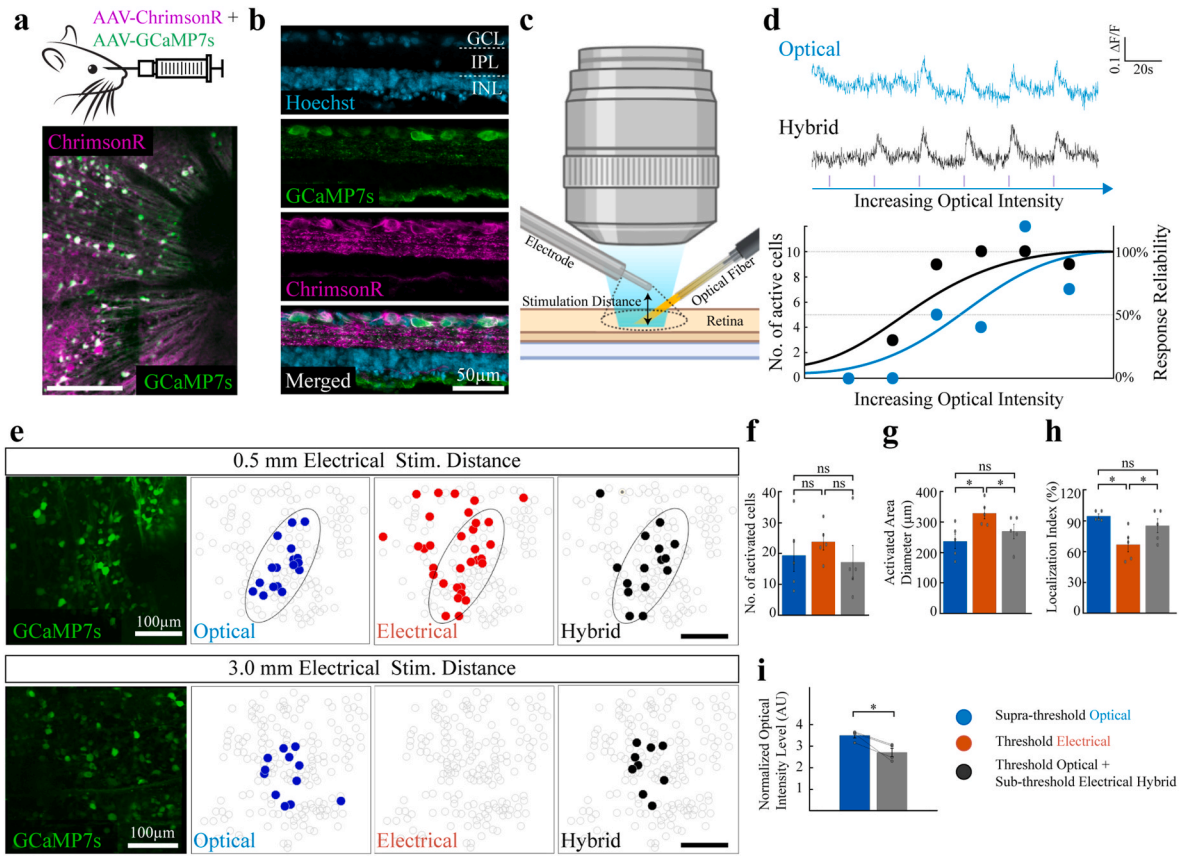

Fig. 4. Hybrid Stimulation of RGCs in Retinae with Inherited Photoreceptor Loss.
(a, b) A viral strategy to transduce RGCs with ChR2 variant ChrimsonR and calcium indicator GCaMP7s in the RCS-p + retina. The absence of somatic expression of ChrimsonR & GCaMP7s in the INL suggests expression is restricted to RGCs. Scale bars in **(a)** and **(b)** are 200 μm and 50 μm respectively. **(c)** Optical stimulation was delivered via an optical fibre with a diameter of 125 μm placed in contact with the GCL. Electrical stimulation was delivered via an epiretinal electrode placed 0.5 mm (n = 5) or 3.0 mm (n = 4) away from the GCL surface. **(d)** Example traces of fluorescent transients of a GCaMP7s+ cell responding to optical-only stimulation and hybrid stimulation with increasing optical intensities. Note that under hybrid conditions, the cell responds to hybrid stimulation at low optical intensity (2nd optical intensity level). The number of activated cells during optical-only and hybrid stimulation at different optical intensity levels. A sigmoidal curve was used to determine activation thresholds, defined as the optical intensity required to reach 50 % response efficacy. The leftward shift in the hybrid stimulation condition (black curve) indicates that hybrid stimulation lowered the optical activation threshold. **(e)** Activation patterns from example retinal explants where extracellular electrical stimulation was delivered at 0.5 mm (top row) and 3.0 mm (bottom row). Calcium dependent activity was recorded from changes in fluorescent signal in GCaMP7s+ RGCs. Activated cells are depicted with coloured filled circles, while inactive cells are shown with open circles. "Optical" refers to optical-only stimulation at a suprathreshold level. "Electrical" refers to electrical-only stimulation at a threshold level. "Hybrid" refers to hybrid stimulation using a combination of threshold optical and sub-threshold electrical stimulation. The ellipses shown under different conditions are identical, representing the area that covers at least 90 % of the activated cells in Optical. This area is used to calculate the localisation index (See Methods). Note that electrical stimulation alone delivered at 3.0 mm did not evoke any GCaMP7s transients. **(f–h)** Population analysis of the five subjects where electrical stimulation was delivered at 0.5 mm using the same conditions shown in **(e)**. The colour scheme employed in population analysis is the same as **(e)**. Mean and standard errors of the mean of the number of cells activated **(f),** the surface area activated **(g)** and the localisation of activation **(h)** are summarised in Tables S15, S18 and S21. Exact p values for the number of cells activated, area activated, and localisation index are summarised in Table S16/17, S19/20, and S22/23 respectively. The number of cells activated under hybrid conditions is comparable to the optical and electrical conditions. The area of activation was significantly greater under the electrical condition when compared with optical (p = 0.043) and hybrid (p = 0.043) as per Wilcoxon Signed-Rank test. The area activated by optical and hybrid stimulation did not differ significantly (p = 0.345). The localisation index further showed the electrical condition was less spatially precise when compared to hybrid (p = 0.043) and optical (p = 0.043) conditions as determined by Wilcoxon Signed-Rank test. The spatial resolution between hybrid and optical conditions was comparable (p = 0.500). **(i)** Hybrid stimulation delivered in the condition where the electrode was 3.0 mm away resulted in an activation pattern that was similar to the optical-only stimulation pattern but this was achieved by using optical intensities that were significantly lower (n = 4, paired *t*-test, p = 0.0175).

3.3. The response reliability of hybrid stimulation surpasses electrical and optical only stimulation

Previous reports have shown that ChR2-H134R can only evoke a maximum firing rate of ~20–40 Hz [13,21]. We investigated whether hybrid stimulation could enhance the response reliability of RGCs at higher stimulation frequencies. We used supra-threshold optical stimulation that elicited response reliability that fell within the top two quartiles (i.e. response reliability >50 %) to ensure that the absence or reduction of responses at higher frequencies was not simply due to insufficient power delivered to the RGC. We coupled the optical stimulation with electrical stimulation at threshold amplitudes (i.e. 50 % response probability) with the rationale that we could leverage the high evoked firing frequency that is characteristic of electrical stimulation, while minimising the effects of electrical spread (Fig. 3a). Given refractory periods in retinal neurons can vary between 1 and 4 ms [56, 57], we had to modify our stimulation pulse widths to be < 5 ms to potentially evoke spike rates that exceed 100 Hz. We therefore employed light pulses with a 1 ms pulse width (Fig. 3b) as used in previous work on the cochlea [31] to determine if increases in response reliability could be achieved using lower power optical pulses (power is proportionate to pulse length at a given intensity). In these experiments,

the electrical stimulus was delayed 1 ms after the onset of the optical pulses, such that it occurred directly after the optical pulse, in order to maximize the facilitation between the stimuli [30,54].

We quantified how a RGC responded to supra-threshold optical-only stimulation, threshold electrical-only stimulation, or hybrid stimulation based on the number of action potentials evoked during a stimulus pulse train. Stimulation was delivered at 2, 20, 50 and 200 Hz for 3 s (Fig. 3c). The responses recorded under the three stimulation modalities at the four frequencies constituted one trial and each cell underwent a minimum of three trials (Fig. 3c and d, another example cell shown in Fig. S1, Tables S5 and S6).

For the 29 RGCs surveyed, response reliability under hybrid conditions was significantly higher throughout the 3 s stimulation pulse train compared to optical or electrical-only modalities. From the onset of the stimulus, RGCs responded prolifically, and their response rate decayed to a steady state for the duration of the stimulation. The decay in response is evident across all three stimulation modalities with the exception of 2 Hz stimulation (Fig. 3e). However, hybrid stimulation was able to sustain a significantly higher response rate at stimulation frequencies of 2–50 Hz (Fig. 3c–f, $p < 0.0001$, see also Tables S7 and S8). The possibility that hybrid stimulation has a more pronounced effect on the excitability or desensitisation in some RGC groups cannot be excluded. Whilst cells from all RGC groups responded reliably to hybrid stimulation at 20 Hz, the enhancement of response reliability varied at 50 Hz particularly in B type RGCs (Tables S2–5).

Critically, from stimulus onset, hybrid stimulation achieved near 100 % response rates at pulse trains up to 50 Hz, a significant enhancement over optical-only or electrical-only stimulation despite significant decay after the first 500 ms (Fig. 3e).

To confirm that neuron firing is precisely controlled by the stimulation, we analysed the latency of the responses and summarised the results in Fig. 3g and Tables S9 and S10. Compared to electrical-only stimulation, optical-only stimulation resulted in longer and more varied response latencies at frequencies ranging from 2 to 50 Hz. Hybrid stimulation significantly reduced the response latencies compared to optical-only stimulation ($p < 0.0001$), although the latencies remained longer than those from electrical-only stimulation. The latency analysis of the recordings from 200 Hz stimulation is less informative, as cells often need more than 5 ms to reach the peak of the first action potential in response to electrical and/or optical stimulation (Fig. 3g).

3.4. Hybrid stimulation can activate RGCs in a degenerated retina with reduced optical power compared to optical-only stimulation

We next determined if the advantages of employing hybrid stimulation that we observed in ChR2(H134R) RGCs are translatable to the degenerated retina. We adopted a Royal College of Surgeons (RCS-p+) rat model. Their genetic defect, characterised by progressive photoreceptor loss [58] is a faithful representation of the hereditary retinopathy retinitis pigmentosa [59]. Previous studies in RCS-p+ rats have demonstrated that despite the complete degeneration of photoreceptors, some of the RGC population is spared and remains functional. However, the physiology is altered with reports of RGCs requiring higher electrical depolarisation thresholds for action potential propagation and reduced spiking. At the late-stage of the disease, RGCs can become unresponsive to electrical stimulation due to the absence of inward sodium currents [60,61].

Therefore, to assess if hybrid stimulation can be implemented as a therapeutic, we needed to determine if hybrid stimulation can drive RGC activity in the degenerated retina at safe power levels and with greater spatial precision than electrical stimulation alone.

To address this aim, we delivered intravitreal injections of AAVs encoding the channelrhodopsin variant ChrimsonR and the genetically encoded calcium indicator GCaMP7s in RCS-p+ rats (Fig. 4a and b). We utilized ChrimsonR, a red-shifted opsin with demonstrated efficacy, safety and long-term stability in the retina of nonhuman primates and improved vision outcomes in a clinical trial [16,18]. We performed patch clamping recordings in individual RGCs expressing ChrimsonR from RCS-p+ rats using the same parameters utilized in the ChR2-H134R mouse RGCs to study the threshold levels ($n = 4$) and the temporal responses ($n = 5$) to hybrid stimulation. The results collected using the diseased model are similar to those obtained from our observations obtained from ChR2-H134R transgenic mice (Figs. S2 and S3). Hybrid stimulation reduced the mean optical thresholds as electrical stimulation levels increased but this wasn't statistically significant in our recordings (One-way ANOVA, $p = 0.0839$). Nevertheless, it did increase the response reliability of RGCS compared to electrical-only or optical-only stimulation at 2 and 20 Hz (Tables S11 and S12).

For the above ChR2-H134R transgenic mouse and ChrimsonR-transduced RCS-p+ rat studies, electrical stimulation was delivered intracellularly via the patch clamping microelectrodes. However, electrical retinal prostheses deliver electrical stimulation extracellularly. Thus, to demonstrate that the principle of hybrid stimulation can be translated for extracellular stimulation, whole-cell patch clamp recordings were collected from one ChrimsonR expressing RCS-p+ rat RGC under whole-cell recording conditions where electrical stimulation was delivered epiretinally. The results were consistent with the results obtained using intracellular electrical stimulation where we observed optical thresholds being attenuated with the supplementation of electricity and more critically, improved response reliability when hybrid stimulation was delivered at 20 Hz and 50 Hz (Fig. S4, Tables S13 and S14).

3.5. Hybrid stimulation with broad electrical stimulation

To explore the spatial resolution of hybrid stimulation, we modified our hybrid stimulation paradigm to target a population of RGCs via extracellular stimulation, which is more clinically realistic compared to intracellular stimulation used in patch clamp recordings. There are numerous approaches for electrode placement in the field of retinal prostheses. Strategies that have been explored include epiretinal (on top of the inner limiting membrane), subretinal (between the pigment epithelium and inner nuclear layer) and suprachoroidal (into the sclera behind the choroid). Suprachoroidal devices are considered less invasive than epiretinal and subretinal implants, but they typically suffer from low spatial resolution due to broad electrical stimulation [62]. We employed near-cell and broad electrical stimulation to simulate the different placements of stimulation electrodes in clinical configurations. In our experiments, hybrid stimulation comprised of electrical stimulation delivered via an extracellular electrode placed epiretinal approximately 0.5 mm ($n = 5$) as well as 3.0 mm ($n = 4$) above the GCL, immediately after focused optogenetic illumination through an optic fibre (Fig. 4c). The range of 0.5–3.0 mm approximates the electrode to retina separation in the suprachoroidal configuration [63]. We hypothesized that hybrid stimulation would not reduce the spatial resolution achievable from focused optogenetic experiments but would reduce the optical power required for stimulation.

Following effective transduction in whole isolated retinal flat mounts (Fig. 4a and b), we stimulated the retina using a combination of electrical and optical stimulation. We first determined the threshold intensities for optical-only and electrical-only stimulation by imaging the RGC responses at different intensities (Fig. 4c and d). Fig. S5 shows changes in the activation pattern at different optical and electrical stimulation levels within the field of view (FOV) in an example retina. In line with the experimental design, optical-only produced localized activation within the FOV, which became more consistent with increased optical intensities, but did not broaden. In contrast, while low-level electrical stimulation was also localized within the FOV, higher electrical stimulation levels resulted in a broader activation area, extending beyond the FOV. We defined the supra-threshold intensities for both optical and electrical stimulation as those beyond which increasing the stimulation amplitudes did not alter the activation

pattern or increase the number of activated cells within the FOV. As electrical stimulation was broad and optical stimulation was focused, the number of cells activated by suprathreshold optogenetic stimulation was smaller compared to suprathreshold electrical stimulation. Interestingly, we did not observe the axon bundle activation during optogenetic stimulation, a challenge often encountered with electrical stimulation of RGCs, which can lead to distorted phosphenes reported by patients [64].

Next, we examined the effects of hybrid stimulation using a total of 15 conditions: 3 levels of optical-only stimulation, 3 levels of electrical-only stimulation, and 9 hybrid electrical-optical combinations (Fig. S6). The maximum optical intensity was set at a supra-threshold level, while the maximum electrical intensity was set at a threshold level. Fig. 4e shows an example retina explant where electrical stimulation is delivered 0.5 mm away and an area of RGCs that are responding to suprathreshold optical-only stimulation (Optical), threshold electrical-only stimulation (Electrical), and hybrid stimulation, where optical stimulation was threshold and electrical stimulation was sub-threshold (Hybrid). This example shows that an equivalent number of activated cells and similar activation patterns can be achieved using lower intensity optical and electrical stimuli.

To further quantitatively assess the impact of hybrid stimulation, we analysed the number and area of RGCs (Fig. 4f and g) that could be activated by hybrid stimulation and compared these responses to electrical and optical-only stimulation modalities at RGCs stimulated with the electrode placed 0.5 mm away. The number of activated cells did not differ significantly among the three conditions (Wilcoxon Signed-Rank Test, $p > 0.05$). Whilst the area of RGCs activated by Hybrid was comparable to Optical, both stimulation conditions activated RGCs within a smaller area, producing more confined activation patterns when compared to Electrical stimulation (Wilcoxon Signed-Rank Test, $p = 0.043$). This suggests that hybrid stimulation can achieve spatial resolution comparable to confined optical-only stimulation, with lower optical intensity requirements.

We also studied the level of localisation for each condition (Fig. 4h). The level of localisation was determined by a localisation index, defined as the percentage of activated cells within a specific area. This area was determined by fitting a 90 % confidence ellipse around the cells activated by the suprathreshold optical-only stimulation. The localisation index was similar between Hybrid and Optical stimulation (Wilcoxon Signed-Rank Test, $p > 0.05$), with both significantly higher than that of Electrical stimulation.

When the distance of electrical stimulation was increased to 3.0 mm, delivery of electricity alone did not evoke responses in RGCs. RGCs could however be activated in the suprathreshold optical-only and hybrid conditions. Whilst the real pattern of activation was similar between the optical-only and hybrid conditions, the number of activated RGCs was achieved with significantly lower optical intensities in the hybrid condition (Fig. 3i, two-tailed paired *t*-test, $p = 0.0175$).

Fig. S7 summarizes the number of activated RGCs, the activation area, as well as the localisation index across 15 combinations of optical and electrical stimulation. Overall, hybrid stimulation increased the number of activated RGCs compared to optical and electrical-only stimulation at equivalent intensity levels. We attribute this increase to a reduction in the activation threshold, which aligns with our findings of lower activation thresholds under hybrid conditions, observed in our whole-cell current-clamp assays (Fig. 2, S2, S4). At a fixed optical stimulation level, the activation area increased with the addition of electrical stimulation, although this measure was less accurate at higher electrical intensities since some activated cells likely extended beyond the FOV. The localisation index was higher for optical-only stimulation compared to electrical-only stimulation. At a fixed optical stimulation level, it decreased with an increase in electrical stimulation level.

We also performed calcium imaging experiments on whole isolated retinal flat mounts ($n = 3$) using a different setup, where more focused epiretinal electrical stimulation and broader optical illumination were applied. In these experiments, we observed a comparable number and area of active cells when using hybrid stimulation at low intensities and single modality stimulation at higher intensities (Fig. S8). These results further suggest that hybrid stimulation can achieve a spatial resolution comparable to that of focused electrical stimulation but with reduced stimulation intensities.

4. Discussion

At the turn of the century, the restoration of vision via a retinal prosthesis became a viable possibility; however, visual acuity remains poor. Clinically, electrical stimulation is still the dominant strategy to restore vision in retinal degeneration [62,64,65], although optogenetic approaches to restore visual function in animal models and humans are beginning to emerge [18,66]. Optogenetic stimulation presents an attractive solution, as the ability to focus light potentially allows for a high level of spatial resolution in neural activation. However, it can be challenging to fully exploit these benefits because the poor temporal properties of many opsins preclude their use in therapeutic applications. A concerted effort has been made towards developing optogenetic constructs with faster kinetics. However, many of these opsins require high light intensities, with a potential negative impact on the welfare of implant recipients. High power intensities can increase the temperature of illuminated tissue which suppresses the physiological firing rate of neurons [67] and at high enough intensities, can lead to phototoxicity [68]. By employing a hybrid opto-electrical strategy, we aimed to determine if such an approach could provide improved spatiotemporal control while driving RGCs with reduced irradiance levels.

Our hybrid stimulation approach reduced RGC activation thresholds compared to electrical stimulation alone, a finding consistent with previous studies in the auditory system. In the mouse, cochlear implants were used to deliver hybrid stimulation to the cochlear spiral ganglion neurons. Using sub-threshold or threshold light, significantly less electrical current was required to activate these neurons [30,31]. In turn, this resulted in less spread of activation in the cochlea, improving the spectral resolution and independence of stimulating channels [31,69]. Perhaps more critically, our hybrid strategy permitted us to photoactivate opsin expressing RGCs with lower levels of irradiance. Electrical supplementation reduced optical thresholds by approximately half and this mechanism could potentially be leveraged with red-shifted opsins, which are already being used in clinical trials, such as ChrimsonR [18]. Whilst hybrid stimulation can significantly reduce optical thresholds, the level of light intensity required for optogenetic activation remains above ambient illumination and is wavelength specific. As such, targeted light delivery rather than relying on natural light conditions is still required for photoactivation.

When we delivered hybrid stimulation to RGCs, response reliability also improved at higher stimulation frequencies when compared to optical-only and electrical-only methods. This again mirrors findings in the cochlea, in which it was shown that hybrid stimulation increased reliability and temporal precision of responses compared to optogenetic stimulation alone [29,30]. We delivered stimulation pulses up to 200 Hz and whilst we did not expect to observe 100 % response reliability at 200 Hz stimulation, we wanted to determine that even with failed action potential propagation with each stimulation pulse, if the evoked response frequency would exceed 20 Hz. In the 200 Hz stimulation condition, hybrid stimulation only evoked a spike rate of ~18 Hz (Table S7). This suggests that with our fixed parameters of 1 ms supra-threshold optical pulses and 3 ms threshold electrical pulse, 20 Hz appears to be the maximum evoked firing frequency, which aligns with previous observations with ChR2 variants in RGCs [70,71]. Although the peak firing rates were still below the 300 Hz burst firing achieved by RGCs with natural light stimulation [72,73], the results reveal that hybrid stimulation enhances the reliability of responses to high frequency stimulation compared to optical-only methods. Our approach enhanced response reliability during hybrid delivery at stimulation

frequencies up to 50 Hz. Most critically we were able to achieve this by employing electrical stimulation at threshold levels and optical stimulation below saturation intensities.

The scope of this study did not permit us to investigate the effect of hybrid stimulation across RGC subtypes on a large scale. Our observations that hybrid stimulation could reduce optical thresholds and improved response reliability in RGCs expressing ChR2-H134R were largely based on recordings in B and C type RGCs. A and D subtypes, which encompass ~10 % and 20 % of all RGCs, respectively, were under-represented in our recordings (n = 4 and n = 1 recorded, respectively). Despite the limited sampling we did observe enhanced response reliability across all RGC subtypes (Tables S2–5). Whilst we did not observe any significant differences in electrical and optical thresholds between RGC groups in our recordings (Table S1), previous large scale physiological studies in the retina show the intrinsic properties can vary greatly across groups [74,75]. In our study we observed hybrid stimulation could increase response reliability in all RGC groups at 20 Hz, but this effect was not as robust during 50 Hz stimulation, especially for B-RGCs (Tables S2–5). Despite the variability in reliability observed between RGC types during 50 Hz stimulation, in clinical presentations, populations of RGCs will be heterogeneous and encompass all RGC subtypes. So while the impact of hybrid stimulation may be less prominent in B type RGCs, significant enhancement in response reliability in just A and C groups could still contribute greatly to vision restoration as these two groups encompass approximately half the total RGC population [52]. Along with the reduction in activation thresholds, hybrid stimulation is primed to be a viable method for RGC activation across the whole retina. This is supported by our recordings in the RCS retina whereby ChrimsonR was expressed pan-neuronally across all RGC subtypes and enhancement of response reliability (Fig. S3) as well as reduction in activation thresholds (Fig. 4) was observed.

Our study did not investigate the biophysics of how hybrid stimulation reduces optical thresholds and improves response reliability in greater detail. However, the extensive physiological examination of the intrinsic properties in neurons expressing ChRs in previous studies does permit us to make meaningful speculations. We hypothesize that the reductions in optical thresholds during hybrid stimulation is underpinned by the opening kinetics as well as the conductance of Na^+ channels and ChRs. Voltage gated Na+ channels possess sub millisecond opening times with rates as fast as 300 μs whilst the ChR2 (H134R) opening rate is ~1.92 ms [25,76,77]. In addition to possessing slow kinetics, ChRs have low Na^+ conductance (~1 pS) when compared to voltage gated Na^+ channels (~17 pS) [25,78]. What this translates to is approximately 500,000 ChRs will need to open simultaneously to depolarize a cell at rest by 15 mV and with 1 ms optical pulses, peak depolarisation occurs after the optical pulse has been delivered [31]. By coupling the electrical pulse with a delay, we can capitalize on the higher conductance of voltage gated Na^+ channels and therefore deliver electrical pulses at lower intensities and more critically, align their opening with the opening times of ChR2-H134R to maximize concurrent inward Na^+ current which could lead to action potential propagation.

Regarding the enhancement in response reliability, ChRs are permeable to all cations, but they do preferentially permit the flow of Na^+ ions over K^+ ions [79] and this mechanism is what permits action potential propagation under optical control. Action potentials in RGCs are driven by Na^+ currents [80] and these inward currents can be evoked by electrical stimulation. However, the amplitude of the Na^+ currents drops significantly at electrical stimulation rates that exceed 50 Hz, and this is reflected in the significant decrease in response reliability [81]. High axonal expression of voltage-gated Na^+ channels Nav1.1 and Nav1.6 has been shown to be the molecular basis that facilitates and sustains high firing rates in neuronal populations such as cortical parvalbumin fast spiking interneurons [82], as well as RGCs [83]. During stimulation under hybrid conditions, the increased response reliability we observed may be due to two mechanisms. The first is that ChR2-H134 expressing RGCs potentially have more Na^+ channels, possessing both native voltage gated Na^+ channels as well as the genetically expressed ChR2-H134R. The availability of more Na^+ channels could conceivably facilitate meeting the somatic thresholds for action potential propagation during higher frequency tetanic stimulation. The second mechanism may be related to how a RGC responds to somatic electrical stimulation and whole-cell optogenetic stimulation. In the electrical modality, stimulation elicits neuronal activity by opening Na^+ channels, however K^+ channels are also concurrently opened. The parallel opening of both Na^+ and K^+ channels has been hypothesized to be one of the mechanisms underpinning reduced response reliability in high frequency electrical stimulation [84]. In the optical modality, stimulation of ChR2 can result in increases in extracellular K^+ by ~5 mM [85] which, depending on location within the nervous system, can be more than twice the amount of extracellular K^+ at physiological rest [86]. Potassium voltage-gated channels are functionally heterogeneous, and whilst Kv3.1/3.2 channels can facilitate fast spiking [87], the Kv1.1 class is involved in suppressing action potentials and neuronal excitability [88]. Regardless of preferred stimulation modality, control of the timing of K^+ channel opening will be an ongoing challenge for the development of any neural interface. Whilst further biophysical interrogation of both electrical and optogenetic stimulation is required to obtain a definitive picture on the temporal limits of exogenous stimulation, we hypothesize that at the core of our hybrid stimulation approach, we are evoking more inward Na^+ currents and, given that our approach utilizes less electricity, we may be reducing the amount of concurrent K^+ channel activation, leading to increased response reliability.

The inability to enhance response reliability at hybrid stimulation frequencies beyond 50 Hz could be attributed to a combination of the biophysical properties of ChR2-H134R and intrinsic properties of RGCs. Although ChR2-H134R has been shown to elicit near 100 % response reliability during 40–60 Hz stimulation in cochlear spiral ganglion neurons [29,31], previous studies that focused on RGC stimulation have shown a reduced response reliability when light pulses were delivered at rates beyond 20 Hz [70,71,89,90]. With the arrival of more robust opsins with faster recovery rates and lower levels of desensitisation such as ChRmine, ChroME variants or PsCatCh 2.0 [14,91,92], replication of high frequency firing should be more attainable. A computational investigation of RGC control under the opsin ChRmine suggests that temporal control can be elicited at rates of up to 280 Hz [93]. If this theoretical temporal bandwidth can be translated to in vivo conditions, it could potentially be further enhanced through a hybrid delivery method. This would be a significant contribution to addressing the technical hurdles of meeting the spatial and temporal precision requirements of retinal prostheses.

From a translational perspective, it is crucial to evaluate the effectiveness of our hybrid approach, which incorporates electrical stimulation delivered extracellularly. Principally, the method of electrical stimulation to evoke neural activity is similar between intracellular and extracellular approaches. Extracellular electrical pulse trains delivered at sufficiently high frequencies and amplitude, targeted at the sodium channel band of RGCs can evoke firing rates >100 Hz [94]. However, extracellular stimulation often activates a network of circuits that leads to activation of local inhibitory neurons, ultimately limiting spiking activity [95]. It has been previously reported that intracellular electrical stimulation of RGCs elicits higher spike rates compared to extracellular stimulation (25 spikes s^{-1} versus 10 spikes s^{-1}) [96]. Furthermore, extracellular electrical stimulation required higher frequencies (~256 Hz versus ~64 Hz to elicit peak firing rate) and current amplitudes (μA versus pA) [96]. The reduced peak firing rates observed through extracellular stimulation may also be due to depolarisation block, a phenomenon where overstimulation results in a decrease in activity. Typically, axons and not cell bodies are activated through electrical stimulation, and this is consistent within the retina [97–99]. The axon is vulnerable to depolarisation block and whilst the precise mechanisms are not fully understood, accumulation of extracellular potassium in the

peri-axonal space is believed to be a significant contributor to perturbed action potential conduction during high frequency stimulation [100,101]. Given the limitations on retinal response reliability with extracellular electrical-only stimulation methods at high frequencies, this further underscores the need to explore alternative methods for manipulating retinal neuron responses.

Encouraged by the temporal and activation threshold improvements achieved by our hybrid strategy, we sought to investigate the therapeutic potential of opto-electrical stimulation in a degenerated retina. We first determined if hybrid stimulation has an effect on thresholds and response reliability at a single cell level in surviving RGCs in the RCS-p + rat. Whilst hybrid stimulation did not induce significant changes in the threshold, response reliability was significantly improved. Interestingly, in our survey at the single cell level, even under hybrid conditions we only achieved a maximum evoked firing rate of ~10 Hz in RCS-p + RGCs. This is considerably less than the maximum firing frequency of 100 Hz that has been reported in nonhuman primate RGCs transduced with ChrimsonR [15]. Potentially, this could be due to RGCs in the degenerated retina of RCS-p + rat exhibiting altered excitability and most notably, reduced maximum firing frequency [102]. Despite our inability to evoke high frequency firing in RGCs, we did demonstrate that hybrid stimulation improves response reliability in the diseased retina compared to electrical or optical only stimulation. To account for potential alterations in RGC excitability in the diseased retina, future pre-clinical studies should focus on exploring opsins with kinetics and photosensitivity beyond that of ChrimsonR.

Thompson and colleagues demonstrated that hybrid stimulation in the cochlea resulted in a reduced spread of activation [31]. The PRIMA implant, which currently provides the highest level of visual restoration, utilizes electrodes with 100 μm diameter, while less invasive suprachoroidal implants would utilize electrode diameters of 600 μm [65]. We speculate that hybrid stimulation might be particularly beneficial when large electrodes are used as these systems also have the largest electrical spread. Therefore, we conducted experiments in a model of retinitis pigmentosa using broad electrical stimulation delivered via electrodes that had effective surface areas of 500 μm in diameter, coupled with highly focused optical stimulation. We observed that the number of activated RGCs, activation area of the retina and localisation index were comparable to optical-only methods, with the additional benefit of reducing the level of irradiance of RGCs. This effect was consistent at electrical stimulation distances of 0.5 mm and 3.0 mm away, suggesting that hybrid stimulation could potentially be translated into systems that don't directly make contact with neurons or neural tissue and as such, exploration of its effects at electrical stimulation distances beyond 3.0 mm is warranted.

Vision restoration through retinal prostheses still faces many hurdles as multiple unresolved questions remain regarding the neural code of the retina. For example, how signals relating to different wavelengths of light are conveyed at the ganglion cell level is still poorly understood although some ground-breaking studies have begun to shed light on how colour perception can be delivered to patients with photoreceptor loss [103,104]. As current devices are only able to provide achromatic vision, accurate object perception will be even more dependent on high spatiotemporal resolution. With the rapid expansion of the genetic toolkit, the hybrid opto-electrical approach could prove critical to the activation of RGCs at the subtype level. Although we could selectively activate remnant RGCs in the diseased retina, for the scope of this study, we did not utilize hybrid stimulation to explore the differences in evoked neural activity in RGCs at the subtype level or separate activation of ON or OFF pathways. The ON and OFF circuits can be disentangled, as each pathway can be identified through its differential responses to electrical stimulation [45,105–107], via tuneable nanoparticles [108], and genetic tools [109,110]. More recently, with the development of AAVs with novel synthetic promoters, neuronal populations within the retina can be differentially targeted with a level of selectivity down to RGC subtype [111]. As the processing of visual features relies on the synergy of different retinal circuits, future explorations of RGC stimulation to restore visual perception should leverage genetic tools that permit the specific targeting of RGC subtypes and segregation of the ON and OFF pathways.

Our results suggest that hybrid stimulation will have broader utility than cochlear and retinal applications. The issue of imprecise activation from electrical stimulation is not exclusive to retinal devices but persists as an issue in vagus nerve stimulation therapies, management of cardiac arrhythmias, and treatments that utilize transcranial electrical stimulation [68,112–114].

Considering implementation in the retinal context, treatment would begin with patients receiving intraocular administration of AAVs encoding opsins. To project light accurately into the retina, GenSight Biologics have developed a device that uses specialised cameras, biomimetic mirrors and computer control. This approach has been used with clinical success [18]. Regarding electrical stimulation of the retina, there are numerous ways this could be achieved [65,115]. Surgical approaches for positioning electrodes can be epiretinal, subretinal and suprachoroidal. Non-surgical approaches have also been developed, and these include transcorneal and transorbital systems [116,117]. Recovery from surgical procedures can come with complications [65] and have an adverse impact on the patient's health and wellbeing. When reviewing patients who received the epiretinal Argus II retinal prosthesis system one-year post-implantation, serious adverse events affected 13 out of the 47 patients surveyed. Nine of the events were in relation to the device, whilst four were a result of the implant procedure. In relation to subretinal devices, such as the PRIMA system [6], although the device is well tolerated, adverse events related to the surgical procedure have been reported due to the increased technical challenges associated with subretinal device implantation [8,118]. Thus, the benefits of reducing the invasiveness of device implantation procedures should not be underestimated. At stimulation distances of 3 mm, we demonstrated the potential for hybrid stimulation to be incorporated into suprachoroidal devices. As both optogenetic strategies [119] and suprachoroidal electrical implants [120] continue to be developed and explored clinically, hybrid stimulation is primed to complement current technologies for vision restoration with reduced invasiveness.

While the hybrid approach may not surpass the highest spatial resolution offered by single modalities, it provides significant potential advantages in terms of lowered thresholds and improved frequency responses, which can translate into enhanced temporal resolution, without significant impact on the spatial resolution. The primary goal of this study was to provide a proof-of-concept on how we can leverage the advantage of minimal invasiveness of optogenetic stimulation to improve the implementation of artificial vision.

In an *in vivo* context, we are optimistic that RGCs could be stimulated with threshold depolarizing current, delivered by suprachoroidal implants, as opposed to electronic implants placed in direct contact with the retina surface. In parallel, devices similar to the GenSight goggles, could simultaneously provide focal optogenetic stimulation. With reduced optical thresholds, response reliability will be significantly improved, which ultimately should improve the quality of artificial vision a patient receives. Potentially hybrid stimulation could be implemented non-invasively where the electrical supplementation comes from transcorneal or transorbital devices. Whilst we should be conscious of the technical challenge of precise delivery of the electrical field to the retina through non-invasive means [117,121], given that our experimental data showed hybrid stimulation with sub-threshold electrical stimulation can still evoke neural activation, incorporating a hybrid approach in currently established transcorneal or transorbital stimulation designs could greatly enhance the number of RGCs that can be activated with greater spatial resolution than what has currently been reported.

There is currently no consensus in the field about which technology - optogenetics or electrical stimulation-is superior. It seems likely that multiple solutions will probably be needed for different patient cohorts.

The proposed hybrid solution thus provides a versatile and potentially superior alternative that combines the benefits of both technologies.

CRediT authorship contribution statement

William C. Kwan: Writing – review & editing, Writing – original draft, Visualization, Validation, Software, Project administration, Methodology, Investigation, Formal analysis, Data curation, Conceptualization. **Emma K. Brunton:** Writing – review & editing, Validation, Software, Project administration, Methodology, Investigation, Formal analysis. **Toon Goris:** Validation, Methodology, Investigation, Formal analysis, Conceptualization. **James M. Begeng:** Investigation, Conceptualization. **Tatiana Kameneva:** Writing – review & editing, Supervision. **Paul R. Stoddart:** Writing – review & editing, Supervision, Conceptualization. **Michael R. Ibbotson:** Writing – review & editing, Supervision, Resources, Project administration, Funding acquisition, Conceptualization. **Rachael T. Richardson:** Writing – review & editing, Resources, Project administration, Methodology, Funding acquisition, Conceptualization. **Wei Tong:** Writing – review & editing, Visualization, Validation, Supervision, Software, Resources, Project administration, Methodology, Investigation, Funding acquisition, Formal analysis, Data curation, Conceptualization.

Code availability

The custom MATLAB code for analysing patch clamping data and calcium imaging data is available on figshare, with access links https://doi.org/10.26188/25941019 and https://doi.org/10.26188/25941133, respectively.

Declaration of competing interest

All authors of this manuscript declare there are no conflicting or competing interests involved with the research outlined in this study.

Acknowledgements

The authors wish to acknowledge the contributions and assistance of A. Brzostowska and S. Kwon for technical support with animal husbandry. We also acknowledge the National Institutes of Health (NIH), Rat Resource and Research Center (RRRC) as the donor of the RCS-p + rat strain. This work was supported by Ideas Grants from the National Health and Medical Research Council (GNT2002523 & GNT2029454). W.T. acknowledges the support from the Australian Research Council via a DECRA Fellowship (DE220100302) and Linkage Grant (LP180100638). W.C.K. acknowledges the support provided by the National Health and Medical Research Council Dora Lush Postgraduate Scholarship (APP1190007). The Australian Regenerative Medicine Institute is supported by grants from the State Government of Victoria and the Australian Government. The Australian College of Optometry provided funding towards this project.

Appendix A. Supplementary data

Supplementary data to this article can be found online at https://doi.org/10.1016/j.brs.2025.103012.

Data availability

Source data are provided with this paper. The patch clamping and calcium imaging data that support the findings of this study are available from the corresponding author upon reasonable request. All other relevant data supporting the key findings of this study are available within the article and its Supplementary Information files or from the corresponding author upon reasonable request.

References

[1] Jonas JB, et al. Visual impairment and blindness due to macular diseases globally: a systematic review and meta-analysis. Am J Ophthalmol 2014;158:808–15.
[2] Bull ND, Martin KR. Concise review: toward stem cell-based therapies for retinal neurodegenerative diseases. Stem Cell 2011;29:1170–5.
[3] Cross N, van Steen C, Zegaoui Y, Satherley A, Angelillo L. Retinitis pigmentosa: burden of disease and current unmet needs. Clin Ophthalmol 2022;1993–2010.
[4] Wang B-Y, et al. Electronic photoreceptors enable prosthetic visual acuity matching the natural resolution in rats. Nat Commun 2022;13:6627.
[5] Finn AP, Grewal DS, Vajzovic L. Argus II retinal prosthesis system: a review of patient selection criteria, surgical considerations, and post-operative outcomes. Clinical ophthalmology; 2018. p. 1089–97.
[6] Palanker D, Le Mer Y, Mohand-Said S, Sahel J-A. Simultaneous perception of prosthetic and natural vision in AMD patients. Nat Commun 2022;13:513.
[7] Muqit MMK, et al. Prosthetic visual acuity with the PRIMA subretinal microchip in patients with atrophic age-related macular degeneration at 4 years Follow-up. Ophthal Sci 2024;4.
[8] Holz FG, et al. Subretinal photovoltaic implant to restore vision in geographic atrophy due to AMD. N Engl J Med 2025.
[9] Ramirez KA, Drew-Bear LE, Vega-Garces M, Betancourt-Belandria H, Arevalo JF. An update on visual prosthesis. Int J Retin Vitr 2023;9:73.
[10] Allen PJ. Retinal prostheses: where to from here? Clin Exp Ophthalmol 2021;49:418–29.
[11] Bansal A, Shikha S, Zhang Y. Towards translational optogenetics. Nat Biomed Eng 2023;7:349–69.
[12] Alekseev A, et al. Efficient and sustained optogenetic control of sensory and cardiac systems. Nat Biomed Eng 2025.
[13] Bi A, et al. Ectopic expression of a microbial-type rhodopsin restores visual responses in mice with photoreceptor degeneration. Neuron 2006;50:23–33.
[14] Chen F, et al. Visual function restoration with a highly sensitive and fast Channelrhodopsin in blind mice. Signal Transduct Targeted Ther 2022;7:104.
[15] Chaffiol A, et al. In vivo optogenetic stimulation of the primate retina activates the visual cortex after long-term transduction. Mol Ther, Methods Clin Dev 2022;24:1–10.
[16] McGregor JE, et al. Optogenetic restoration of retinal ganglion cell activity in the living primate. Nat Commun 2020;11:1703.
[17] Gauvain G, et al. Optogenetic therapy: high spatiotemporal resolution and pattern discrimination compatible with vision restoration in non-human primates. Commun Biol 2021;4:125.
[18] Sahel J-A, et al. Partial recovery of visual function in a blind patient after optogenetic therapy. Nat Med 2021;27:1223–9.
[19] Ferrari U, et al. Towards optogenetic vision restoration with high resolution. PLoS Comput Biol 2020;16:e1007857.
[20] Klapoetke NC, et al. Independent optical excitation of distinct neural populations. Nat Methods 2014;11:338–46.
[21] Sengupta A, et al. Red-shifted channelrhodopsin stimulation restores light responses in blind mice, macaque retina, and human retina. EMBO Mol Med 2016;8:1248–64.
[22] Grossman N, et al. In: 2011 annual international conference of the. IEEE Engineering in Medicine and Biology Society; 2011. p. 4167–70.
[23] Schmidt TM, et al. A role for melanopsin in alpha retinal ganglion cells and contrast detection. Neuron 2014;82:781–8.
[24] Jepson LH, et al. High-fidelity reproduction of spatiotemporal visual signals for retinal prosthesis. Neuron 2014;83:87–92.
[25] Lin JY. A user's guide to channelrhodopsin variants: features, limitations and future developments. Exp Physiol 2011;96:19–25.
[26] Lin JY, Lin MZ, Steinbach P, Tsien RY. Characterization of engineered channelrhodopsin variants with improved properties and kinetics. Biophys J 2009;96:1803–14.
[27] Mager T, et al. High frequency neural spiking and auditory signaling by ultrafast red-shifted optogenetics. Nat Commun 2018;9:1750.
[28] Wäldchen S, Lehmann J, Klein T, Van De Linde S, Sauer M. Light-induced cell damage in live-cell super-resolution microscopy. Sci Rep 2015;5:15348.
[29] Ajay EA, et al. Auditory nerve responses to combined optogenetic and electrical stimulation in chronically deaf mice. J Neural Eng 2023;20:026035.
[30] Hart WL, et al. Combined optogenetic and electrical stimulation of auditory neurons increases effective stimulation frequency—an in vitro study. J Neural Eng 2020;17:016069.
[31] Thompson AC, et al. Hybrid optogenetic and electrical stimulation for greater spatial resolution and temporal fidelity of cochlear activation. J Neural Eng 2020;17:056046.
[32] Richardson RT, et al. Viral-mediated transduction of auditory neurons with opsins for optical and hybrid activation. Sci Rep 2021;11:11229.
[33] Matarazzo JV, et al. Combined optogenetic and electrical stimulation of the sciatic nerve for selective control of sensory fibers. Front Neurosci 2023;17:1190662.
[34] Kim MJ, et al. Hybrid electro-optical stimulation improves ischemic brain damage by augmenting the glymphatic System. Adv Sci 2025;12:2417449.
[35] Roh H, Kang J, Lee HM, Im M. Enhanced optogenetic stimulation of retinal ganglion cells with assistive electric stimulation for low optical power artificial vision. IEEE Trans Neural Syst Rehabil Eng 2025;33:1958–68.
[36] Puthussery T, Fletcher E. Extracellular ATP induces retinal photoreceptor apoptosis through activation of purinoceptors in rodents. J Comp Neurol 2009;513:430–40.

[37] Edelstein AD, et al. Advanced methods of microscope control using μManager software. J Biol l Methods 2014;1:e10.
[38] Hamill OP, Marty A, Neher E, Sakmann B, Sigworth FJ. Improved patch-clamp techniques for high-resolution current recording from cells and cell-free membrane patches. Pflügers Archiv 1981;391:85–100.
[39] Guo T, et al. Mediating retinal ganglion cell spike rates using high-frequency electrical stimulation. Front Neurosci 2019;13:413.
[40] Soto-Breceda A, Kameneva T, Meffin H, Maturana M, Ibbotson M. Irregularly timed electrical pulses reduce adaptation of retinal ganglion cells. J Neural Eng 2018;15:056017.
[41] Schindelin J, et al. Fiji: an open-source platform for biological-image analysis. Nat Methods 2012;9:676–82.
[42] Famiglietti Jr E, Kolb H. Structural basis for ON-and OFF-center responses in retinal ganglion cells. Science 1976;194:193–5.
[43] Dana H, et al. High-performance calcium sensors for imaging activity in neuronal populations and microcompartments. Nat Methods 2019;16:649–57.
[44] Thévenaz P, Unser M. User-friendly semiautomated assembly of accurate image mosaics in microscopy. Microsc Res Tech 2007;70:135–46.
[45] Yunzab M, et al. Preferential modulation of individual retinal ganglion cells by electrical stimulation. J Neural Eng 2022;19:045003.
[46] Tong W, et al. Improved visual acuity using a retinal implant and an optimized stimulation strategy. J Neural Eng 2019;17:016018.
[47] Hendrickson A, Possin D, Kwan W, Huang J, Bourne JA. The temporal profile of retinal cell genesis in the marmoset monkey. J Comp Neurol 2016;524:1193–207.
[48] Lee BB, Martin PR, Grünert U. Retinal connectivity and primate vision. Prog Retin Eye Res 2010;29:622–39.
[49] Kim T-J, Jeon C-J. Morphological classification of parvalbumin-containing retinal ganglion cells in mouse: single-cell injection after immunocytochemistry. Investig Ophthalmol Vis Sci 2006;47:2757–64.
[50] Kovács-Öller T, et al. Spatial expression pattern of the major Ca2+-Buffer proteins in mouse retinal ganglion cells. Cells 2020;9:792.
[51] Goetz J, et al. Unified classification of mouse retinal ganglion cells using function, morphology, and gene expression. Cell Rep 2022;40.
[52] Sun W, Li N, He S. Large-scale morphological survey of mouse retinal ganglion cells. J Comp Neurol 2002;451:115–26.
[53] Sanes JR, Masland RH. The types of retinal ganglion cells: current status and implications for neuronal classification. Annu Rev Neurosci 2015;38:221–46.
[54] Duke AR, et al. Combined optical and electrical stimulation of neural tissue in vivo. J Biomed Opt 2009;14. 060501-060501-060503.
[55] Delori FC, Webb RH, Sliney DH. Maximum permissible exposures for ocular safety (ANSI 2000), with emphasis on ophthalmic devices. J Opt Soc Am A 2007;24:1250–65.
[56] Nirenberg S, Carcieri SM, Jacobs AL, Latham PE. Retinal ganglion cells act largely as independent encoders. Nature 2001;411:698–701.
[57] Oesch N, Euler T, Taylor WR. Direction-Selective dendritic action potentials in rabbit retina. Neuron 2005;47:739–50.
[58] Adachi K, et al. Optical coherence tomography of retinal degeneration in royal college of surgeons rats and its correlation with morphology and electroretinography. PLoS One 2016;11:e0162835.
[59] Strauss O, Stumpff F, Mergler S, Wienrich M, Wiederholt M. The royal college of surgeons rat: an animal model for inherited retinal degeneration with a still unknown genetic defect. Cells Tissues Organs 1998;162:101–11.
[60] Chen Z, Song Y, Yao J, Weng C, Yin ZQ. Alterations of sodium and potassium channels of RGCs in RCS rat with the development of retinal degeneration. J Mol Neurosci 2013;51:976–85.
[61] Ren Y-M, Weng C-H, Zhao C-J, Yin Z-Q. Changes in intrinsic excitability of ganglion cells in degenerated retinas of RCS rats. Int J Ophthalmol 2018;11:756.
[62] Weiland JD, Walston ST, Humayun MS. Electrical stimulation of the retina to produce artificial vision. Annual Rev Vision Sci 2016;2:273–94.
[63] Ayton L, et al. Decrease in electrode-retina distance over time and its effect on electrical impedances in a suprachoroidal retinal prosthesis. Investig Ophthalmol Vis Sci 2013;54:1058. 1058.
[64] Tong W, Meffin H, Garrett DJ, Ibbotson MR. Stimulation strategies for improving the resolution of retinal prostheses. Front Neurosci 2020;14:262.
[65] Ayton LN, et al. An update on retinal prostheses. Clin Neurophysiol 2020;131:1383–98.
[66] Pan Z-H, Lu Q, Bi A, Dizhoor AM, Abrams GW. Optogenetic approaches to restoring vision. Annual Rev Vision Sci 2015;1:185–210.
[67] Owen SF, Liu MH, Kreitzer AC. Thermal constraints on in vivo optogenetic manipulations. Nat Neurosci 2019;22:1061–5.
[68] Richardson RT, Ibbotson MR, Thompson AC, Wise AK, Fallon JB. Optical stimulation of neural tissue. Healthcare Tech Lett 2020;7:58–65.
[69] Azees AA, et al. Spread of activation and interaction between channels with multi-channel optogenetic stimulation in the mouse cochlea. Hear Res 2023;440:108911.
[70] Degenaar P, et al. Optobionic vision—a new genetically enhanced light on retinal prosthesis. J Neural Eng 2009;6:035007.
[71] Pan Z-H, Ganjawala TH, Lu Q, Ivanova E, Zhang Z. ChR2 mutants at L132 and T159 with improved operational light sensitivity for vision restoration. PLoS One 2014;9:e98924.
[72] Margolis DJ, Detwiler PB. Different mechanisms generate maintained activity in ON and OFF retinal ganglion cells. J Neurosci 2007;27:5994–6005.
[73] Uzzell V, Chichilnisky E. Precision of spike trains in primate retinal ganglion cells. J Neurophysiol 2004;92:780–9.
[74] O'Brien BJ, Isayama T, Richardson R, Berson DM. Intrinsic physiological properties of cat retinal ganglion cells. J Physiol 2002;538:787–802.
[75] Wong RCS, Cloherty SL, Ibbotson MR, O'Brien BJ. Intrinsic physiological properties of rat retinal ganglion cells with a comparative analysis. J Neurophysiol 2012;108:2008–23.
[76] Schmidt-Hieber C, Bischofberger J. Fast sodium channel gating supports localized and efficient axonal action potential initiation. J Neurosci 2010;30:10233–42.
[77] Vanoye CG, Lossin C, Rhodes TH, George Jr AL. Single-channel properties of Human NaV1.1 and mechanism of channel dysfunction in SCN1A-associated epilepsy. J Gen Physiol 2005;127:1–14.
[78] Baker MD, Bostock H. Inactivation of macroscopic late Na+ current and characteristics of unitary late Na+ currents in sensory neurons. J Neurophysiol 1998;80:2538–49.
[79] Deisseroth K, Hegemann P. The form and function of channelrhodopsin. Science 2017;357. eaan5544.
[80] Lipton SA, Tauck DL. Voltage-dependent conductances of solitary ganglion cells dissociated from the rat retina. J Physiol 1987;385:361–91.
[81] Tsai D, Morley JW, Suaning GJ, Lovell NH. Frequency-dependent reduction of voltage-gated sodium current modulates retinal ganglion cell response rate to electrical stimulation. J Neural Eng 2011;8:066007.
[82] Hu H, Gan J, Jonas P. Fast-spiking, parvalbumin+ GABAergic interneurons: from cellular design to microcircuit function. Science 2014;345:1255263.
[83] Van Wart A, Matthews G. Impaired firing and cell-specific compensation in neurons lacking nav1. 6 sodium channels. J Neurosci 2006;26:7172–80.
[84] Cameron MA, et al. Differential effect of brief electrical stimulation on voltage-gated potassium channels. J Neurophysiol 2017;117:2014–24.
[85] Octeau JC, et al. Transient, consequential increases in extracellular potassium ions accompany channelrhodopsin2 excitation. Cell Rep 2019;27:2249–2261. e2247.
[86] Moghaddam B, Adams RN. Regional differences in resting extracellular potassium levels of rat brain. Brain Res 1987;406:337–40.
[87] Kuznetsov KI, Grygorov OO, Maslov VY, Veselovsky NS, Fedulova SA. Kv3 channels modulate calcium signals induced by fast firing patterns in the rat retinal ganglion cells. Cell Calcium 2012;52:405–11.
[88] Chi XX, Nicol GD. Manipulation of the potassium channel Kv1. 1 and its effect on neuronal excitability in rat sensory neurons. J Neurophysiol 2007;98:2683–92.
[89] Lin C-I, Chiao C-C. Blue light promotes neurite outgrowth of retinal explants in postnatal ChR2 mice. eNeuro 2019;6.
[90] Tomita H, et al. Channelrhodopsin-2 gene transduced into retinal ganglion cells restores functional vision in genetically blind rats. Exp Eye Res 2010;90:429–36.
[91] Marshel JH, et al. Cortical layer–specific critical dynamics triggering perception. Science 2019;365. eaaw5202.
[92] Sridharan S, et al. High-performance microbial opsins for spatially and temporally precise perturbations of large neuronal networks. Neuron 2022;110:1139–1155.e1136.
[93] Bansal H, Gupta N, Roy S. Theoretical analysis of optogenetic spiking with ChRmine, bReaChES and CsChrimson-expressing neurons for retinal prostheses. J Neural Eng 2021;18:0460b0468.
[94] Cai C, Ren Q, Desai NJ, Rizzo JF, Fried SI. Response variability to high rates of electric stimulation in retinal ganglion cells. J Neurophysiol 2011;106:153–62.
[95] Crapper DR, Noell WK. Retinal excitation and inhibition from direct electrical stimulation. J Neurophysiol 1963;26:924–47.
[96] Kotsakidis R, Meffin H, Ibbotson MR, Kameneva T. In vitro assessment of the differences in retinal ganglion cell responses to intra-and extracellular electrical stimulation. J Neural Eng 2018;15:046022.
[97] Fried SI, Lasker AC, Desai NJ, Eddington DK, Rizzo 3rd JF. Axonal sodium-channel bands shape the response to electric stimulation in retinal ganglion cells. J Neurophysiol 2009;101:1972–87.
[98] Nowak L, Bullier J. Axons, but not cell bodies, are activated by electrical stimulation in cortical gray matter I. Evidence from chronaxie measurements. Exp Brain Res 1998;118:477–88.
[99] Nowak L, Bullier J. Axons, but not cell bodies, are activated by electrical stimulation in cortical gray matter II. Evidence from selective inactivation of cell bodies and axon initial segments. Exp Brain Res 1998;118:489–500.
[100] Kameneva T, et al. Retinal ganglion cells: mechanisms underlying depolarization block and differential responses to high frequency electrical stimulation of ON and OFF cells. J Neural Eng 2016;13:016017.
[101] Shin D, et al. High frequency stimulation or elevated K+ depresses neuronal activity in the rat entopeduncular nucleus. Neuroscience 2007;149:68–86.
[102] R. Yi-Ming, W. Chuan-Huang, Z. Cong-Jian, Y. Zheng-Qin, Changes in intrinsic excitability of ganglion cells in degenerated retinas of RCS rats. Int J Ophthalmol 11, 756-765.
[103] Paknahad J, Loizos K, Yue L, Humayun MS, Lazzi G. Color and cellular selectivity of retinal ganglion cell subtypes through frequency modulation of electrical stimulation. Sci Rep 2021;11:5177.
[104] Yue L, Castillo J, Gonzalez AC, Neitz J, Humayun MS. Restoring color perception to the blind: an electrical stimulation strategy of retina in patients with end-stage retinitis pigmentosa. Ophthalmology 2021;128:453–62.
[105] Hadjinicolaou AE, Cloherty SL, Hung Y-S, Kameneva T, Ibbotson MR. Frequency responses of rat retinal ganglion cells. PLoS One 2016;11:e0157676.
[106] Madugula SS, et al. Focal electrical stimulation of human retinal ganglion cells for vision restoration. J Neural Eng 2022;19:066040.
[107] Muralidharan M, et al. Neural activity of functionally different retinal ganglion cells can be robustly modulated by high-rate electrical pulse trains. J Neural Eng 2020;17:045013.
[108] Begeng JM, et al. Activity of retinal neurons can be modulated by tunable near-infrared nanoparticle sensors. ACS Nano 2023;17:2079–88.

[109] Cronin T, et al. Efficient transduction and optogenetic stimulation of retinal bipolar cells by a synthetic adeno-associated virus capsid and promoter. EMBO Mol Med 2014;6:1175–90.
[110] Lu Q, et al. AAV-mediated transduction and targeting of retinal bipolar cells with improved mGluR6 promoters in rodents and primates. Gene Ther 2016;23:680–9.
[111] Jüttner J, et al. Targeting neuronal and glial cell types with synthetic promoter AAVs in mice, non-human primates and humans. Nat Neurosci 2019;22:1345–56.
[112] Bortoletto M, Rodella C, Salvador R, Miranda PC, Miniussi C. Reduced current spread by concentric electrodes in transcranial electrical stimulation (tES). Brain Stimul 2016;9:525–8.
[113] Entcheva E, Kay MW. Cardiac optogenetics: a decade of enlightenment. Nat Rev Cardiol 2021;18:349–67.
[114] Harris AR. Current perspectives on the safe electrical stimulation of peripheral nerves with platinum electrodes. Bioelectron Med 2020;3:37–49.
[115] Palanker D. Electronic retinal prostheses. Cold Spring Harb Perspect Med 2023; 13:a041525.
[116] Fujikado T, et al. Effect of transcorneal electrical stimulation in patients with nonarteritic ischemic optic neuropathy or traumatic optic neuropathy. Jpn J Ophthalmol 2006;50:266–73.
[117] Lee S, Park J, Kwon J, Kim DH, Im C-H. Multi-channel transorbital electrical stimulation for effective stimulation of posterior retina. Sci Rep 2021;11:9745.
[118] Wu KY, Mina M, Sahyoun J-Y, Kalevar A, Tran SD. Retinal prostheses: engineering and clinical perspectives for vision restoration. Sensors 2023;23:5782.
[119] Mohanty SK, et al. A synthetic opsin restores vision in patients with severe retinal degeneration. Mol Ther 2025;33:2279–90.
[120] Lombardi L, et al. Face and available chair detection and localization with a second-generation (44-Channel) suprachoroidal retinal prosthesis. Transl Vis Sci Technol 2025;14:11. 11.
[121] Lu Z, et al. An in-silico analysis of retinal electric field distribution induced by different electrode design of trans-corneal electrical stimulation. J Neural Eng 2022;19:055004.